Vacuum 243 (2026) 114841

Contents lists available at ScienceDirect

Vacuum

journal homepage: www.elsevier.com/locate/vacuum

First-principles study of K_2XH_4 (X= Mg, Ca) hydrides: structural, mechanical, and optoelectronic aspects for hydrogen storage applications

Abdullah Candan [a,*], Salih Akbudak [b]

[a] Department of Machinery and Metal Technology, Kirsehir Ahi Evran University, Kirsehir, 40100, Turkey
[b] Vocational School of Health Services, Adiyaman University, 02040, Adiyaman, Turkey

ARTICLE INFO

Keywords:
DFT
Desorption temperature
Phonon
Hydrogen storage
HSE06
Optoelectronics

ABSTRACT

Perovskite-type hydrides have emerged as promising solid-state hydrogen storage materials owing to their high volumetric density and safety. Motivated by this potential, Density Functional Theory (DFT) and Ab Initio Molecular Dynamics (AIMD) simulations were performed to investigate the structural, optoelectronic, thermodynamic, mechanical, and hydrogen storage properties of K_2XH_4 (X = Mg, Ca) hydrides. Specifically, phonon dispersion and negative formation enthalpies indicate that both compounds are dynamically and thermodynamically stable. Moreover, AIMD simulations performed for 5000 fs confirm their thermal stability, showing no structural distortion during the simulation. Electronic structure calculations reveal wide band gap semiconducting behavior: 3.43 eV for K_2MgH_4 and 3.41 eV for K_2CaH_4 within GGA-PBE, further increased to 4.67 eV and 4.60 eV with HSE06. From a mechanical perspective, elastic constants satisfy the Born stability criteria, confirming mechanical stability, while Pugh's ratio and Cauchy pressure suggest brittle behavior. Optical analyses indicate strong activity in the UV region. Regarding hydrogen storage, gravimetric capacities (desorption temperatures) were calculated as 3.80 wt% (207.87 K) for K_2MgH_4 and 3.30 wt% (254.88 K) for K_2CaH_4. Overall, K_2MgH_4 appears suitable for moderate hydrogen storage, whereas K_2CaH_4 is more favorable for applications requiring structural resilience and efficient hydrogen release.

1. Introduction

For decades, fossil fuels have formed the foundation of the global energy supply. However, their use leads to serious environmental and climatic issues [1–5]. In particular, the combustion of fossil fuels releases large amounts of greenhouse gases, primarily carbon dioxide, which accelerates global warming, drives climate change, and causes irreversible damage to natural ecosystems [6]. To mitigate climate change and ensure environmental sustainability, low-carbon alternative energy solutions, such as solar energy, hydrogen energy, and other renewable resources, are urgently needed [7–9]. Among these options, hydrogen energy is especially attractive because of its high efficiency, environmental purity, and the possibility of production from renewable sources [10,11]. Unlike fossil fuels, the combustion of hydrogen generates only water vapor, which improves air quality and offers a significant advantage in combating climate change. In addition to hydrogen storage, considerable attention has been devoted to hydrogen production via the hydrogen evolution reaction (HER) [12–14]. For example, Pan and Gao [12] investigated transition-metal-doped V_2C MXene electrocatalysts and found that doping weakens V–C bond interactions, facilitates hydrogen desorption, and enhances optical responses from the UV to the visible range. Similarly, Yang et al. [13] studied borophene-based single-atom catalysts, demonstrating excellent catalytic activity for HER. Furthermore, Yang et al. [14] reported that noble-metal doping in borophene/WS_2 heterojunctions substantially improves catalytic performance, underscoring their strong potential for practical HER applications.

Several studies have also demonstrated that hydrogen can be used as a fuel in vehicles without producing harmful emissions [15–17]. Current research, therefore, prioritizes the development of efficient and reliable hydrogen storage systems. Due to their unique structural and physical characteristics, alkali- and alkaline-earth-based complex hydrides have emerged as important candidates for hydrogen storage applications. These materials, comprising hydrogen-rich compounds such as $[AlH_4]^-$, $[BH_4]^-$ or $[ZnH_4]^{2-}$ formed with light alkali (Li, Na, K) or alkaline-earth metals (Mg, Ca, Sr), are attractive because of their high hydrogen content, low molar mass, and tunable thermodynamic and kinetic properties [18–21]. Within this framework, Pan and Yang [22] explored

* Corresponding author.
E-mail address: acandan@ahievran.edu.tr (A. Candan).

https://doi.org/10.1016/j.vacuum.2025.114841
Received 20 June 2025; Received in revised form 10 October 2025; Accepted 18 October 2025
Available online 19 October 2025

Li–N–H hydrides, showcasing their potential for hydrogen storage and notable optical characteristics. Furthermore, Pan and Gao [23] investigated the storage and dehydrogenation mechanisms of $AMMgH_3$ (AM = Li, Na, K, and Rb) hydrides. Recently, Gao et al. [24] emphasized the promise of $X_3N_3H_6$ (X = B, C, and Al) hydrides, noting their high gravimetric capacity and significant UV absorption, thereby expanding the possibilities within the realm of hydrogen-rich complex hydrides. Collectively, these studies demonstrate the adaptability of complex hydrides and provide important perspectives on their various structural forms. Various crystal structures, such as ABH_4, A_2BH_4, and A_2MH_6, have been identified within this class, enabling the customization of hydrogen release and uptake behavior. Numerous investigations have confirmed that these materials offer significant potential for hydrogen storage, with advantages including high gravimetric capacity, structural and dynamic stability, favorable kinetic properties, and high volumetric hydrogen density [25–28]. Beyond storage, complex hydrides also show promise for applications involving optical, thermoelectric, and other functional properties [29–34].

Bertheville et al. [35] structurally characterized K_2MgH_4 as a tetragonal K_2NiF_4-type compound (*I4/mmm*), with lattice parameters a = 4.0361 Å, c = 13.5921 Å, and c/a = 3.37. Neutron diffraction studies revealed that the Mg-centered octahedra are compressed along the tetragonal axis, indicating a distinct structural anisotropy. In a recent experimental study, Rodenburg et al. [36] highlighted that K_2MgH_4 is not only a stable hydride but also exhibits mixed hydride–electronic conductivity. Bertheville et al. also documented the successful synthesis of novel Cs- and Mg-based ternary hydrides (i.e., $CsMgH_3$, $Cs_4Mg_3H_{10}$, and Cs_2MgH_4) by reacting stoichiometric mixtures of binary hydrides under thermal conditions, highlighting the versatility of Mg-containing complex hydrides [29]. These materials are significant due to their inclusion of $[MgH_6]^{4-}$ octahedral anionic motifs, presenting a viable alternative to conventional $[MgH_4]^{2-}$ tetrahedral structures by improving volumetric hydrogen storage capacity. Wang et al. conducted first-principles calculations employing the generalized gradient approximation to investigate the same compounds, revealing significant bandgap insulating properties and a dominant ionic character governed by the $[MgH_6]^{4-}$ octahedral units [30]. These findings are complemented by the recent work of Liu et al. [37], which systematically investigated the structural, mechanical, and optoelectronic properties of $X_3H(ZnH_4)$ (X = Na, K, Rb, Cs) hydrides. Their results revealed wide band gaps, strong ultraviolet absorption, and promising hydrogen storage capacities, thereby highlighting the potential of these compounds for future energy-related applications. According to Ahmed et al. [32], Cs_2CaH_4 and Rb_2CaH_4 not only exhibit stable tetragonal structures but also demonstrate promising hydrogen storage capacities and favorable electronic properties, making them attractive candidates for practical hydrogen storage systems where stability and minimal electronic interference are crucial. In another theoretical study, Yamcicier carefully looked at the structural, electronic, and vibrational properties of tetragonal X_2MgH_4 (X = K, Rb, Cs) compounds using density functional theory [26]. It was further noted that all three compounds are stable according to the Born stability criterion and are dynamically stable, with hydrogen storage capacities of 3.8 wt% for K_2MgH_4, 2.02 wt% for Rb_2MgH_4, and 1.37 wt% for Cs_2MgH_4. Similarly, Rehman and colleagues conducted first-principles studies on X_2ZnH_4 (X = K, Rb, Cs) compounds and demonstrated that their structural, electronic, thermal, and mechanical properties were favorable [38]. These compounds also demonstrate potential for hydrogen storage, as they can hold moderate amounts of hydrogen with capacities of 2.7 wt% for K_2ZnH_4, 1.6 wt% for Rb_2ZnH_4, and 1.2 wt% for Cs_2ZnH_4.

According to the literature, K_2MgH_4 crystallizes in a tetragonal structure, is elastically anisotropic and brittle, and exhibits insulating character with no imaginary phonon modes, confirming its vibrational stability. However, no prior studies have reported on the K_2CaH_4 crystal, leaving a significant gap in the field of complex metal hydride-based hydrogen storage. To the best of our knowledge, this work represents the first comprehensive investigation of K_2CaH_4, while also extending the understanding of K_2MgH_4. Building on the earlier GGA-PBE study, the present work employs hybrid functionals (HSE06) for more accurate electronic and optical descriptions and incorporates additional analyses, including AIMD-based thermal stability, Bader charge distribution, and zero-point energy corrections. A detailed assessment of the structural, thermodynamic, mechanical, electronic, optical, and vibrational properties of K_2XH_4 (X = Mg, Ca) offers theoretical insights into their stability, energy efficiency, and hydrogen storage potential. The results demonstrate that both compounds exhibit dynamic and thermodynamic stability together with favorable hydrogen storage characteristics, positioning them as strong candidates for renewable energy systems.

2. Methodology

This research examined the essential physical features of K_2XH_4 (X = Mg, Ca) hydrides, including mechanical, dynamic properties, and hydrogen storage capacity, using density functional theory (DFT). All computations were performed with the VASP (Vienna Ab initio Simulation Package) [39,40], using the Projector Augmented Wave (PAW) method [41] for the electron–ion interactions. The valence electron configurations were set as $1s^2\ 2s^2\ 2p^6\ 3s^2\ 3p^6\ 4s^1$ for K, $1s^2\ 2s^2\ 2p^6\ 3s^2$ for Mg, $1s^2\ 2s^2\ 2p^6\ 3s^2\ 3p^6\ 4s^2$ for Ca, and $1s^1$ for H. The Generalized Gradient Approximation (GGA) functional was used for the exchange-correlation energy, specifically using the Perdew-Burke-Ernzerhof (PBE) formulation [42]. Since the GGA-PBE approach usually underestimates the band gap, the optoelectronic properties of K_2XH_4 (X = Mg, Ca) hydrides were investigated using the more accurate Heyd-Scuseria-Ernzerhof (HSE06) exchange-correlation functional [43]. In the geometric optimization procedure, the energy convergence threshold was established at 10^{-8} eV/atom, and the plane wave cut-off energy was set at 600 eV. A 12 × 12 × 4 k-point mesh is used to sample the first Brillouin zone to guarantee the precision of electronic structure computations [44]. Elastic constants are determined with the stress–strain methodology implemented in VASP software [45]. Phonon calculations were performed via the PHONOPY code [46], while ab initio molecular dynamics (AIMD) simulations at 300 K were carried out to assess thermal stability.

To investigate the optical behavior of K_2XH_4 (X = Mg, Ca), the complex dielectric function $\varepsilon(\omega)$ was employed, which is a fundamental parameter describing the interaction of a material with electromagnetic radiation. It consists of the real part $\varepsilon_1(\omega)$, representing dispersion, and the imaginary part $\varepsilon_2(\omega)$, associated with absorption. These components are connected through the Kramers–Kronig relations [47], allowing for a detailed analysis of frequency-dependent optical responses, consistent with recent DFT-based optical studies [48,49]. Based on $\varepsilon(\omega)$, other important optical parameters can be derived, including the optical conductivity $\sigma(\omega)$, refractive index $n(\omega)$, absorption coefficient $I(\omega)$, reflectivity $R(\omega)$, and energy loss function $L(\omega)$. Mathematical formulations are presented in Eqs. (1)–(6):

$$\varepsilon(\omega) = \varepsilon_1(\omega) + i\varepsilon_2(\omega) \tag{1}$$

$$\sigma(\omega) = -\frac{i\omega}{4\pi}\,\varepsilon(\omega) \tag{2}$$

$$n(\omega) = \left[\frac{\sqrt{\varepsilon_1^2(\omega) + \varepsilon_2^2(\omega)} + \varepsilon_1(\omega)}{2}\right]^{1/2} \tag{3}$$

$$I(\omega) = \left[\frac{\sqrt{\varepsilon_1^2(\omega) + \varepsilon_2^2(\omega)} - \varepsilon_1(\omega)}{2}\right]^{1/2} \tag{4}$$

$$R(\omega) = \left|\frac{\sqrt{\varepsilon(\omega)} - 1}{\sqrt{\varepsilon(\omega)} + 1}\right|^2 \tag{5}$$

$$L(\omega) = \frac{\varepsilon_2(\omega)}{\varepsilon_1^2(\omega) + \varepsilon_2^2(\omega)} \quad (6)$$

3. Results and discussions

3.1. Structural properties

The K_2XH_4 (X = Mg, Ca) hydrides crystallize in a tetragonal structure belonging to the space group *I4/mmm* (No. 139) [26]. As illustrated in Fig. 1, the three-dimensional crystal structure of K_2XH_4 reveals that X atoms form the skeleton of the lattice and are positioned at the (0, 0, 0) coordinates. Hydrogen atoms occupy two different crystallographic positions: H_1 atoms are located at (0.5, 0, 0) and H_2 atoms are located at (0.5, 0.5, 0.34), while K atoms are positioned at (0.5, 0.5, 0.16). To determine the equilibrium structural parameters, the total energy of the system was calculated as a function of unit cell volume and subsequently optimized. The calculated energy–volume data were fitted using the Birch–Murnaghan equation of state [50], from which the equilibrium lattice constants, Bulk modulus (B), and its pressure derivative (B′) were extracted. The obtained curves are shown in Fig. 2 for (a) K_2MgH_4 and (b) K_2CaH_4.

Table 1 summarizes the calculated lattice parameters (*a* and *c*), Bulk modulus (*B*), pressure derivative (*B′*), unit cell volume (*V*), formation enthalpy (ΔH_f), and cohesive energy (E_c) for both compounds. For K_2MgH_4, the optimized lattice parameters are a = 4.044 Å and c = 13.636 Å, which are in very good agreement with the experimental and theoretical values reported in the literature (*a* = 4.036 Å, c = 13.592 Å [35]; *a* = 4.049 Å, c = 13.633 Å [36]; *a* = 4.043 Å, c = 13.630 Å [26]). For K_2CaH_4, the optimized lattice constants were computed as *a* = 4.396 Å and c = 14.076 Å. The minor differences between the present calculations and experimental data can be attributed to the use of exchange–correlation functionals within DFT.

Formation energy, one of the basic criteria in determining thermodynamic stability, reflects the energy change that occurs during the synthesis of a compound from its constituent elements. A negative value indicates that the compound is thermodynamically stable, and the synthesis process is energetically favorable. Formation energy, which plays an important role in evaluating the stability of the K_2XH_4 (X = Mg, Ca) compound, can be calculated using the equation given below [28,51,52]:

$$\Delta H_f = \frac{1}{(n_K + n_X + n_{H_2})} \left[E_t(K_2XH_4) - 2E_t(K) - E_t(X) - 2E_t(H_2)\right] \quad (7)$$

The formation energy (ΔH_f) of the K_2XH_4 (X = Mg, Ca) compounds is calculated based on the difference between the total energy of the system $E_t(K_2XH_4)$ and the energies of the component elements in their reference states. $E_t(K)$ and $E_t(X)$ represent the total energy of elements in their bulk ground states, while $E_t(H_2)$ represents the total energy of the hydrogen molecule, respectively. In addition, the symbols n_K, n_X, and n_{H_2} indicate the number of K, X, and H_2 atoms in the unit cell. As can be seen in Table 1, the calculated formation enthalpies are negative for both compounds, with values of −0.283 eV/atom for K_2MgH_4 and −0.347 eV/atom for K_2CaH_4. These negative values indicate that both hydrides are thermodynamically stable and can be spontaneously formed from their constituent elements.

The cohesive energy (E_c) is an important parameter widely used in evaluating the stability of a system. A higher positive cohesive energy implies enhanced structural stability of the crystal. The following formula was used in cohesive energy calculations for this compound [51]:

$$E_c = -\frac{1}{7}\left[E_t(K_2XH_4) - 2E_K - E_X - 2E_{H_2}\right] \quad (8)$$

Here, E_t denotes the total energy contained in a given unit cell and E_K, E_X, and E_{H_2} are the energies of the atoms in isolated form. The cohesive energies obtained for K_2XH_4 (X = Mg, Ca) compounds, as listed in Table 1, further confirm their structural stability. For K_2MgH_4, the cohesive energy is 2.754 eV/atom, while for K_2CaH_4 it is 2.866 eV/atom. These positive values indicate that both compounds possess strong interatomic bonds and robust crystal structures. Such characteristics make K_2MgH_4 and K_2CaH_4 attractive candidates for hydrogen storage applications.

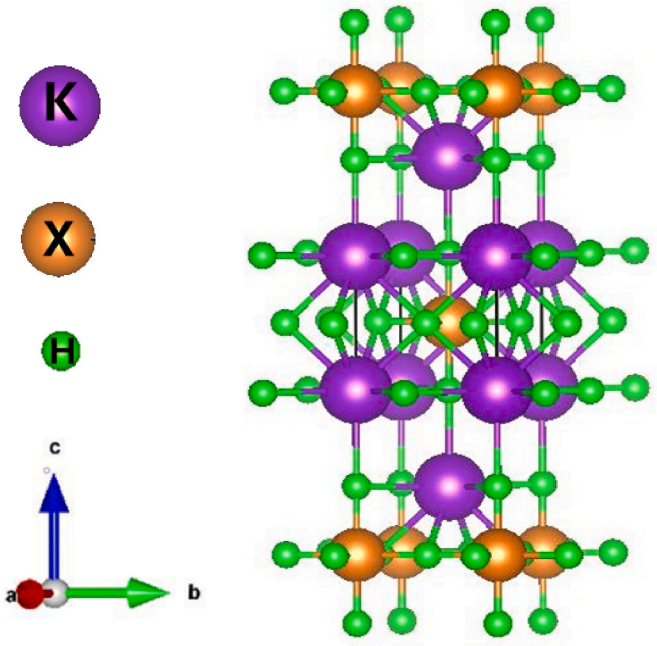

Fig. 1. The three-dimensional crystal structure of K_2XH_4 (X = Mg, Ca).

3.2. Hydrogen storage properties

To evaluate the potential of the K_2CaH_4 compound in hydrogen storage applications, the gravimetric hydrogen storage capacity C_{wt} (%) for the studied compound was calculated using the following formula [53], and the results are given in Table 2:

$$C_{wt}(\%) = \left(\frac{\left(H/M\right) m_H}{m_{host} + \left(H/M\right) m_H} \times 100\right)\% \quad (9)$$

Here, H/M represents the ratio of hydrogen atoms to the parent material, m_{host} and m_H represent the respective molar masses of the host material and hydrogen. The gravimetric hydrogen storage capacity of K_2CaH_4 was determined as 3.30 wt%, while that of K_2MgH_4 was calculated as 3.80 wt% (Table 2). These values indicate that both compounds can store a relatively large amount of hydrogen per unit mass compared to many alkali and alkaline-earth metal hydrides reported in the literature. Specifically, their gravimetric capacities are considerably higher than those reported for Rb_2MgH_4 (2.02 wt%) [26], Cs_2MgH_4 (1.37 wt%) [26], Rb_2SnH_4 (2.77 wt%) [28], Rb_2CaH_4 (1.86 wt%) [32], and Cs_2CaH_4 (1.28 wt%) [32], demonstrating a clear advantage of K-based hydrides over Rb- and Cs-based analogues. This enhancement can be attributed to the lower atomic weight of potassium compared to rubidium and cesium, which increases the hydrogen-to-mass ratio of the compounds. Although the gravimetric hydrogen storage capacities of K_2MgH_4 and K_2CaH_4 are still below the ultimate target of 5.5 wt% set by the U.S. Department of Energy (DOE) for 2025 [54], they nevertheless approach the range considered promising for lightweight solid-state hydrides. Such results emphasize the beneficial role of alkali metal selection in optimizing hydrogen storage properties and highlight K_2MgH_4 and

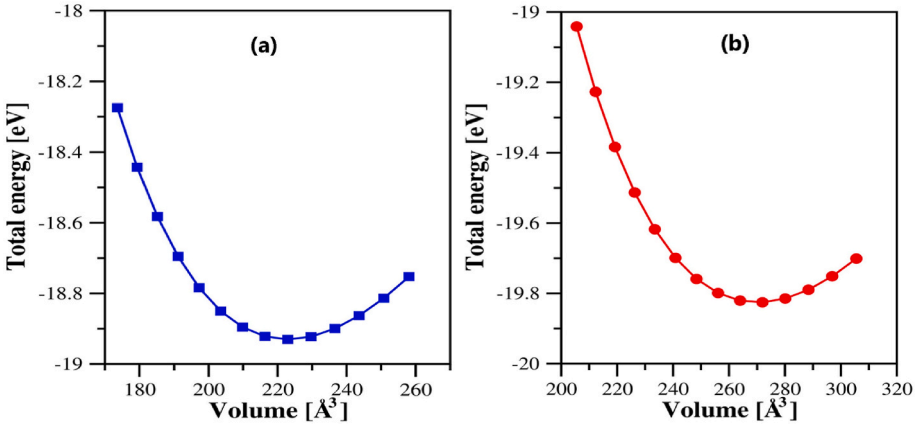

Fig. 2. The optimized total energy-volume curve for (a) K_2MgH_4 and (b) K_2CaH_4.

Table 1
The calculated lattice parameters (*a* and c), Bulk modulus (B), pressure derivative of the Bulk modulus (B'), volume of the unit cell (V), formation enthalpy (ΔH_f), and cohesive energy (E_c) for K_2XH_4 (X = Mg, Ca).

Material	*a* (Å)	*c* (Å)	***B*** (GPa)	***B'***	*V* (Å^3)	ΔH_f (eV/atom)	E_c (eV/atom)	*Ref.*
K_2MgH_4	4.044	13.636	25.90	3.72	222.949	−0.283	2.754	This work
	4.036	13.592	–	–	221.400	–	–	[35-Exp.]
	4.049	13.633	–	–	223.570	–	–	[36-Exp.]
	4.043	13.630	–	–	222.789	–	–	[26]
K_2CaH_4	4.396	14.076	27.95	3.78	272.091	−0.347	2.866	This work

Table 2
The gravimetric (C_{wt}) and volumetric (ρ_{vol}) hydrogen storage capacity, desorption temperatures (T_{des}) of K_2XH_4 (X = Mg, Ca) hydrides.

Material	C_{wt} (%)	ρ_{vol} (g.H_2/L)	T_{des} (K)	*Ref.*
K_2MgH_4	3.80	60.10	207.87	This work
K_2MgH_4	3.80	–	–	[26]
Rb_2MgH_4	2.02	–	–	[26]
Cs_2MgH_4	1.37	–	–	[26]
K_2CaH_4	3.30	49.21	254.88	This work
Rb_2SnH_4	2.77	–	–	[28]
Rb_2CaH_4	1.86	–	101.30	[32]
Cs_2CaH_4	1.28	–	135.67	[32]

K_2CaH_4 as potential candidates for further modification strategies (e.g., doping, nanostructuring, or composite formation) aimed at achieving the DOE targets.

Volumetric hydrogen storage capacity (ρ_{vol}) expresses how much hydrogen a material can store per unit volume and is defined by the following general formula [55]:

$$\rho_{vol} = \frac{N_H \times m_H}{V\,(L) \times N_A} \tag{10}$$

Here, N_H represents the number of absorbed hydrogens, m_H represents the molar mass of hydrogen, V (L) represents the total absorbed volume, and N_A represents Avogadro's number. According to the calculations made within the scope of this study, the volumetric hydrogen storage capacity of the K_2CaH_4 compound was found to be 49.21 g H_2/L, while that of K_2MgH_4 was calculated as 60.10 g H_2/L (Table 2). Both values clearly exceed the U.S. Department of Energy (DOE) 2025 ultimate target of 40 g H_2/L for volumetric capacity [56,57]. These findings demonstrate that K_2CaH_4 and K_2MgH_4 not only meet but surpass the minimum DOE requirements, highlighting their promising potential for practical hydrogen storage. In particular, the higher volumetric capacity of K_2MgH_4 suggests its superior performance in applications requiring compact storage, such as the fuel systems of modern hydrogen-powered vehicles and other space-limited energy storage technologies.

In addition to the gravimetric hydrogen capacity, the determination of the hydrogen desorption temperature (T_{des}) of a hydride is of great importance for hydrogen storage applications. The thermodynamic behavior of hydrides is usually explained by the standard Gibbs free energy, and this relationship is expressed by the following equation [58]:

$$\Delta G = \Delta H - T_{des}.\Delta S \tag{11}$$

In this equation, ΔG represents the Gibbs free energy, ΔH represents the enthalpy of formation, and ΔS represents the entropy change in the system. The change of entropy for hydrogen is accepted as approximately ΔS (H_2) ≈ 130.7 J/mol K [59]. The desorption temperature is defined as the temperature at which the Gibbs free energy is zero. Starting from this point, the desorption temperature was calculated using the following equation [60], and these results are presented in Table 2.

$$T_{des} = -\frac{\Delta H}{\Delta S} \tag{12}$$

As a result of the calculations, the desorption temperature for the K_2CaH_4 compound was determined as 254.88 K, which falls within the optimum operating temperature window of 233–333 K, thereby supporting its usability in practical hydrogen storage systems [61]. In contrast, the desorption temperature of K_2MgH_4 was calculated as 207.87 K, which is slightly below the optimum range. This lower value indicates that hydrogen release is thermodynamically more favorable, offering advantages such as reduced energy demand during desorption and improved overall storage efficiency. Comparison with the literature data (Table 2) further shows that both K_2CaH_4 and K_2MgH_4 exhibit higher desorption temperatures than those reported for Rb_2CaH_4 (101.30 K) [32] and Cs_2CaH_4 (135.67 K) [32]. These findings demonstrate that K-based hydrides not only surpass many Rb- and Cs-based analogues in terms of gravimetric and volumetric capacities but also exhibit more favorable hydrogen release characteristics, making them attractive candidates for solid-state hydrogen storage.

3.3. Mechanical properties

Determination of elastic constants is a critical step in analyzing the mechanical behavior and performance of a material. These quadratic constants characterize the elastic response of the material under tension, revealing its resistance to deformation. They also play a key role in understanding the fundamental properties of the material, such as its hardness and mechanical stability [62]. K_2XH_4 (X = Mg, Ca) compounds with a tetragonal crystal system are characterized by six independent elastic constants: C_{11}, C_{12}, C_{13}, C_{33}, C_{44}, and C_{66}. The numerical values of the calculated elastic constants of this compound are presented in Table 3. The obtained results were used to evaluate both the elastic and mechanical stability of K_2XH_4 (X = Mg, Ca). This evaluation is based on the Born elastic stability criteria. These criteria are the mathematical conditions that determine whether a crystal is elastically stable or not. According to the Born-Huang criteria, a tetragonal crystal must satisfy the following inequality conditions to be considered mechanically stable [62,63].

$$C_{11} > 0, C_{33} > 0,\ C_{44} > 0,\quad C_{66} > 0,\ \ C_{11} > |C_{12}|, 2C_{13}{}^2 < C_{33}(C_{11} + C_{12}) \tag{13}$$

Since K_2MgH_4 and K_2CaH_4 hydrides satisfy these conditions, it can be concluded that both compounds are elastically stable. For K_2MgH_4, the obtained values are in good agreement with the previously reported data in the literature [26], confirming the reliability of the present calculations.

For a material with a tetragonal crystal structure, the Cauchy pressure (C_P) is defined as the difference between the elastic constants C_{12} and C_{66}, and this relationship is mathematically expressed as $C_{12} - C_{66}$. This parameter provides important information about the mechanical behavior of the material. A positive Cauchy pressure usually indicates a ductile structure, while a negative value reflects brittle character [64–66]. As presented in Table 3, the calculated Cauchy pressure of −6.21 GPa for K_2CaH_4 suggests a tendency toward brittleness, while the value of −13.33 GPa for K_2MgH_4 indicates an even stronger brittle character. Furthermore, the obtained results for K_2MgH_4 are in good agreement with previously reported literature data [26], which supports the reliability of the present calculations.

For a comprehensive analysis of the mechanical properties of these compounds, key parameters including Bulk modulus (B), Shear modulus (G), Young's modulus (E), B/G ratio, and Poisson's ratio (ν) were calculated using the Voigt–Reuss–Hill method [67–69] and are summarized in Table 4.

For K_2CaH_4, the Bulk modulus of 22.03 GPa indicates relatively low resistance to volumetric compression, suggesting a less rigid structure. The Shear modulus of 14.79 GPa shows that the compound can withstand deformation within a certain elastic limit but lacks high rigidity. The Young's modulus of 36.25 GPa suggests that K_2CaH_4 is a medium-hard material capable of maintaining structural integrity under tensile stress.

In comparison, K_2MgH_4 exhibits slightly higher values, with a Bulk modulus of 24.25 GPa, a Shear modulus of 18.25 GPa, and a Young's modulus of 43.77 GPa. These values indicate improved resistance to volume compression, shear deformation, and tensile stress compared to K_2CaH_4. For both compounds, the order of elastic moduli (G < B < E) reveals that they are more susceptible to shear deformation than volumetric deformation, providing useful insights into their mechanical stability [70].

Table 4
The calculated values of Bulk modulus (B), Shear modulus (G), Young's modulus (E), B/G, and Poisson's ratio (ν) for K_2XH_4 (X = Mg, Ca).

Compound	B (GPa)	G (GPa)	E (GPa)	B/G	ν	*Ref.*
K_2MgH_4	24.25	18.25	43.77	1.32	0.19	This work
	22.49	17.51	41.70	1.28	0.19	[26]
K_2CaH_4	22.03	14.79	36.25	1.49	0.226	This work

The Pugh ratio (B/G) is a basic mechanical indicator used to evaluate the ductility or brittleness properties of materials and is defined as the ratio of the Bulk modulus (B) to the Shear modulus (G) [71]. Generally, materials with a Pugh ratio greater than 1.75 are classified as ductile, indicating that the material can undergo high levels of plastic deformation before fracture. This ratio below 1.75 indicates a brittle character. According to the results presented in Table 4, the B/G ratio of 1.49 for the K_2CaH_4 compound clearly reveals its brittle nature. Similarly, the B/G ratio of 1.32 obtained for K_2MgH_4 also indicates brittleness, in agreement with Pugh's criteria. These findings are further supported by the calculated Cauchy pressures, which are −6.21 GPa for K_2CaH_4 and −13.33 GPa for K_2MgH_4, confirming that both compounds exhibit brittle behavior.

The Poisson ratio (ν) is an important mechanical parameter used to understand the changes in shape and volume of a material during elastic deformation [72]. However, this ratio also provides valuable information about the type of atomic bonding in the material. For example, a Poisson ratio of around 0.1 indicates that covalent bonds predominate between atoms in the crystal structure, while Poisson ratio values around 0.25 indicate the presence of ionic bonds. Poisson ratios between 0.3 and 0.5 are generally associated with weaker interactions, such as metallic bonds. As shown in Table 4, Poisson's ratio of 0.226 obtained for the compound K_2CaH_4 reveals that ionic bonds predominate between atoms in this crystal. In comparison, Poisson's ratio of 0.19 calculated for K_2MgH_4 also indicates a predominantly ionic bonding nature, consistent with the brittle behavior inferred from the B/G ratio and Cauchy pressure values.

3.4. Electronic properties

Electronic band structure calculations are of critical importance in determining whether a material is conductive, semiconducting, or insulating, depending on the band gap value. The band gap is defined by the energy difference between the highest occupied and lowest unoccupied bands, taking the Fermi level ($E_F = 0$) as a reference. The electronic properties of the alkali metal hydrides K_2XH_4 (X = Mg, Ca) were calculated using both the GGA-PBE [42] and HSE06 [43] approaches, and their electronic band structures were obtained along the high symmetry points Z–Γ–X–P–Γ–N [26], as illustrated in Figs. 3 and 4. The Fermi energy level is shown with dotted lines at 0 eV. Within the GGA-PBE scheme, the band gaps of K_2CaH_4 (3.43 eV) and K_2MgH_4 (3.41 eV) fall into the classification of wide band gap semiconductors (2–4 eV) [73,74]. These values are in excellent agreement with a previous GGA-PBE-based report on related hydrides [26], confirming the reliability of the present calculations. However, the use of the more accurate HSE06 functional increases the band gap values to 4.67 eV for K_2CaH_4 and 4.60 eV for K_2MgH_4, shifting their electronic nature closer to insulating behavior. This functional dependence highlights the sensitivity of electronic structure predictions to the choice of

Table 3
Elastic constants (C_{ij}) and Cauchy pressure (C_P) for K_2XH_4 (X = Mg, Ca).

Material	C_{11} (GPa)	C_{12} (GPa)	C_{13} (GPa)	C_{33} (GPa)	C_{44} (GPa)	C_{66} (GPa)	C_P (GPa)	*Ref.*
K_2MgH_4	51.73	14.37	11.95	40.27	15.40	27.70	−13.33	This work
	47.05	12.84	11.39	38.27	15.38	26.68	–	[26]
K_2CaH_4	46.84	7.84	11.59	42.59	12.85	14.05	−6.21	This work

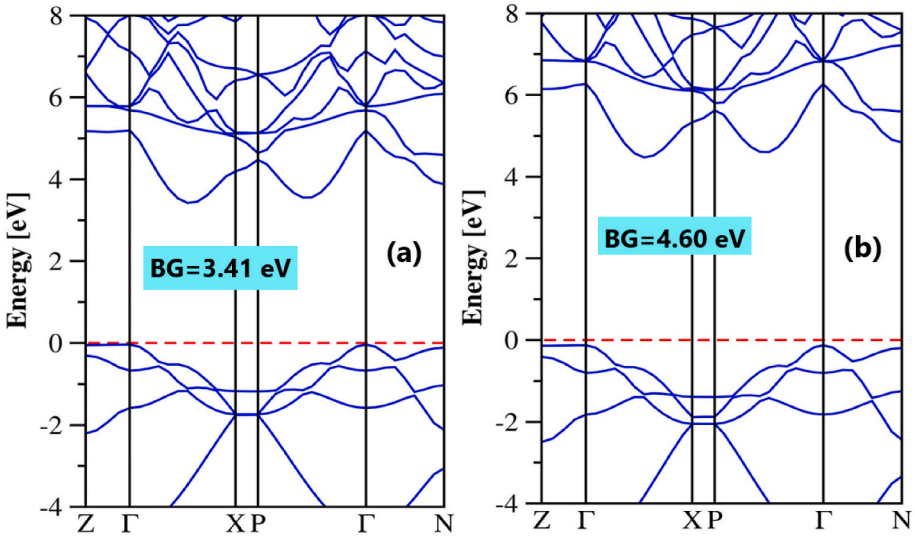

Fig. 3. The electronic band structure of K_2MgH_4 using (a) GGA-PBE and (b) HSE06 functionals.

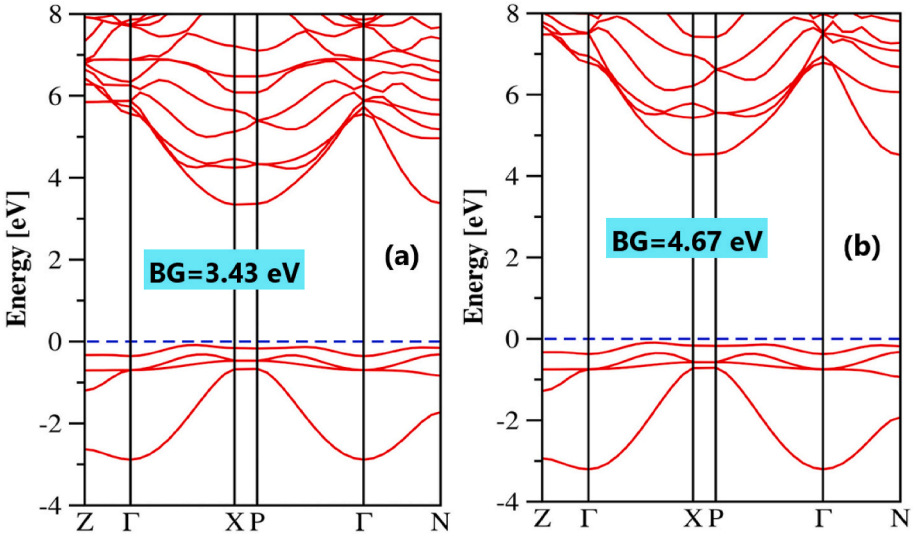

Fig. 4. The electronic band structure of K_2CaH_4 using (a) GGA-PBE and (b) HSE06 functionals.

exchange–correlation approximation and indicates that these compounds may exhibit properties at the boundary between wide band gap semiconductors and insulators. Such characteristics suggest that their potential applications may extend beyond hydrogen storage to other areas of energy and electronics. Wide band gap semiconductors and insulators are advantageous due to their high optical transparency,

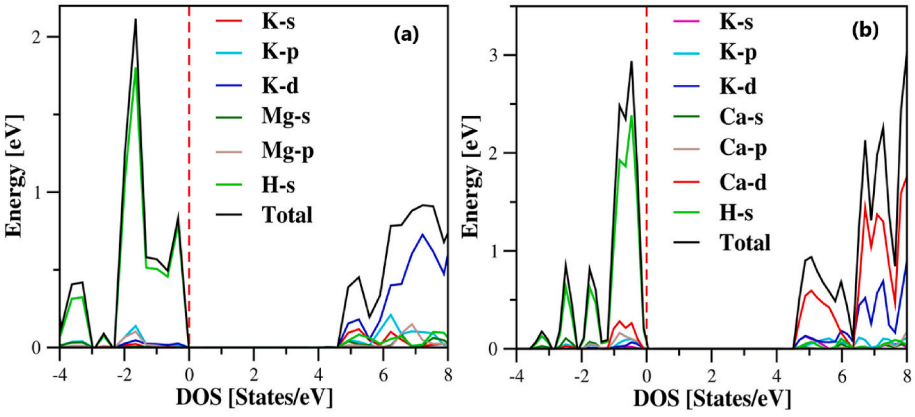

Fig. 5. The TDOS and PDOS of (a) K_2MgH_4 and (b) K_2CaH_4 using HSE06.

tunable electrical conductivity, and controllable carrier density, as well as their resistance to high temperature, voltage, and frequency conditions. Therefore, both K_2CaH_4 and K_2MgH_4 emerge as promising candidates for various optoelectronic devices, particularly UV photodetectors [74].

To further investigate the electronic properties of K_2CaH_4 and K_2MgH_4, total density of states (TDOS) and partial density of states (PDOS) analyses were performed using the HSE06 functional. Fig. 5 illustrates the calculated TDOS and PDOS data, with the red dashed line indicating the Fermi level. The obtained density of states plots are consistent with the band structure diagrams, further confirming that both compounds exhibit electronic properties close to the insulating region as predicted by the HSE06 functional. For K_2CaH_4, the analysis of the valence band shows that the largest contributions to the TDOS arise from the p- and d-orbitals of Ca and the s-orbitals of H, whereas the conduction band is mainly dominated by the d-orbitals of K and Ca. Similarly, for K_2MgH_4, the valence band is largely governed by the s-orbitals of H and the p-orbitals of Mg and K, while the conduction band contributions are primarily associated with the d-orbitals of K. In both compounds, prominent PDOS peaks are observed just below the Fermi level (between −1 eV and 0 eV), reflecting strong orbital hybridization between the alkali metal (K), the alkaline-earth element (Ca or Mg), and hydrogen atoms. This orbital hybridization plays a fundamental role in shaping the electronic structure of the hydrides and directly influences their conductivity, stability, and hydrogen storage properties [75].

3.5. Bader charge analysis

The charge density distributions of these compounds were obtained, and the result for K_2MgH_4 is presented in Fig. 6. As can be seen, the K_2MgH_4 compound exhibits a pronounced ionic bonding character, which is also consistent with its Poisson's ratio. To determine the charge state of each ion in the compounds, Bader partial charge analysis was performed, and the results are summarized in Table 5. The Bader charges were calculated using the VASP package and analyzed with the algorithm developed by Henkelman and co-workers [76], which is based on Bader's approach of zero-flux surfaces [77]. As shown in Table 5, K and X (Mg or Ca) atoms donate positive charges, while hydrogen atoms gain negative charges, clearly indicating the occurrence of charge transfer between ions [78]. For K_2MgH_4, the K and Mg atoms carry net charges of +0.76 and + 1.58 e, respectively, whereas the H atoms acquire approximately −0.77 e. Similarly, for K_2CaH_4, the Bader analysis reveals that K and Ca atoms possess net charges of +0.78 and + 1.43 e, while hydrogen atoms carry approximately −0.75 e. This distribution indicates that roughly 3 electrons per formula unit is transferred into the hydrogen sublattice, confirming the typical hydride nature of these compounds. Furthermore, the K–H interaction is predominantly ionic, whereas a limited covalent contribution is present in the Ca–H bonds. These findings provide important insights into how hydrogen is stabilized within the host lattice and clarify the interaction mechanism between hydrogen and the surrounding metal atoms. Overall, the results are consistent with the charge density distribution, supporting the dominant ionic bonding nature of K_2XH_4 (X = Mg, Ca) compounds.

Table 5
Bader partial charges (in units of electron) for K_2XH_4 (X = Mg, Ca).

Compound	*Atom*			
	K	X	H (1)	H (2)
K_2MgH_4	0.763	1.581	−0.767	−0.787
K_2CaH_4	0.780	1.430	−0.747	−0.748

3.6. Optical properties

Optical properties offer significant potential for improving and optimizing hardware performance in many advanced technology areas such as photonics, optoelectronics, solar energy conversion, sensor systems, and hydrogen storage technologies [78–80]. In this regard, an in-depth understanding of the interactions between hydrogen-based materials and solar radiation plays a critical role both in increasing the efficiency of hydrogen storage systems and in developing innovative material designs. On the other hand, examining the optical properties of hydrogen-related materials is an important step in revealing the fundamental physical mechanisms of these interactions and in understanding the responses of these materials to electromagnetic wave spectra. Such analyses are valuable for both theoretical and applied research. Complex hydrides based on alkaline-earth metals, especially K_2XH_4 (X = Mg, Ca), are of great interest owing to their distinctive structural and electronic characteristics. To understand the optical behavior of such materials in detail, extensive theoretical calculations have been carried out on various optical parameters such as dielectric function, conductivity, reflectivity, and loss function.

Figs. 7 and 8 present the calculated optical response functions of K_2XH_4 (X = Mg, Ca). Fig. 7 shows (a) the real $\varepsilon_1(\omega)$ and (b) imaginary $\varepsilon_2(\omega)$ parts of the dielectric function, (c) the real and (d) the imaginary parts of optical conductivity $\sigma(\omega)$, while Fig. 8 illustrates (a) the refractive index $n(\omega)$, (b) the absorption coefficient $I(\omega)$, (c) the reflectivity $R(\omega)$, and (d) the loss function $L(\omega)$.

The real part of the dielectric function $\varepsilon_1(\omega)$ quantifies the material's polarization response to an external electromagnetic field [81]. As

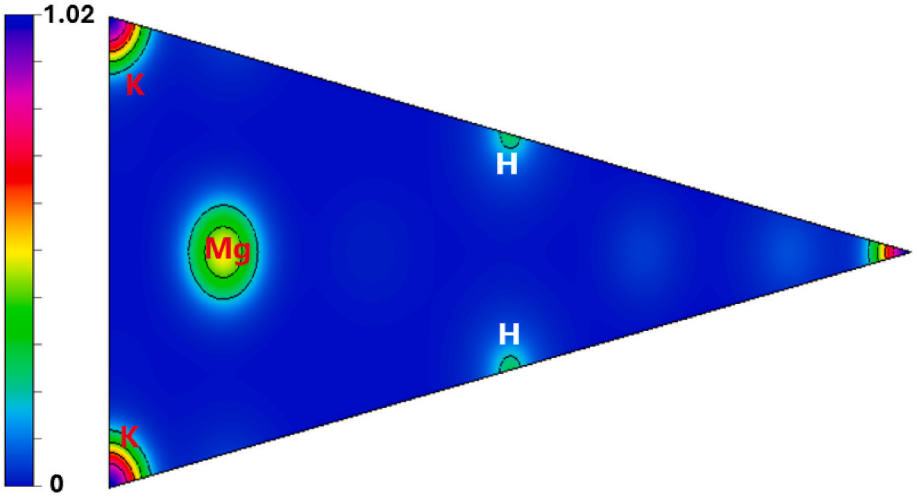

Fig. 6. The charge density distribution of K_2MgH_4.

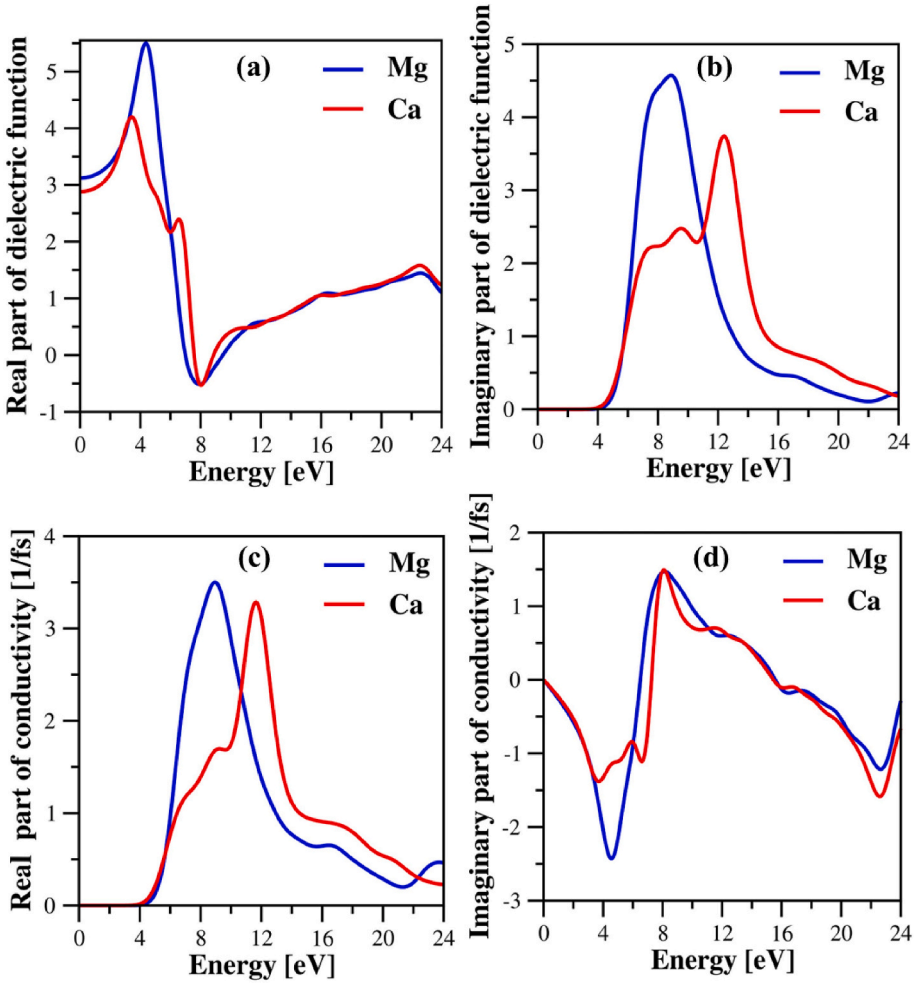

Fig. 7. (a) Real and (b) imaginary part of dielectric function, (c) real and (d) imaginary part of conductivity for K_2XH_4 (X = Mg, Ca).

shown in Fig. 7(a), the static dielectric constant is $\varepsilon_1(0) = 2.88$ for K_2CaH_4 and 3.12 for K_2MgH_4. $\varepsilon_1(\omega)$ increases with increasing photon energy, reaching maxima of 4.19 at 3.44 eV for K_2CaH_4 and 5.49 at 4.36 eV for K_2MgH_4. Fig. 7(b) shows the imaginary dielectric function for K_2XH_4 (X = Mg, Ca). For both compounds, $\varepsilon_2(\omega)$ remains low in the range of 0–4.50 eV, indicating the absence of significant optical transitions in this range and an optically passive response. This behavior is consistent with the onset of the interband transition around 4.5 eV. At higher energies, $\varepsilon_2(\omega)$ increases sharply, showing prominent peaks of 3.74 at 12.40 eV for K_2CaH_4 and 4.57 at 8.87 eV for K_2MgH_4, reflecting intense interband transitions activated by high-energy photons.

When a material is exposed to light, the response of carrier electrons to an external electric field is defined as optical conductivity $\sigma(\omega)$ [81]. This property reflects the material's tendency to acquire electrical conductivity in the presence of light. The real and imaginary parts of the optical conductivity of K_2XH_4 (X = Mg, Ca) compounds are presented in the energy range of 0–24 eV in Fig. 7(c) and (d), respectively. As shown in Fig. 7(c), the real part of the optical conductivity starts to increase at around 4.50 eV for both compounds, indicating the onset of interband optical transitions in K_2XH_4. The real part reaches a maximum of 3.50 1/fs at 8.88 eV for K_2MgH_4 and 3.28 1/fs at 11.59 eV for K_2CaH_4. At higher energies, the values gradually decrease and approach zero. The imaginary part of the optical conductivity, shown in Fig. 7(d), exhibits more complex behavior. For K_2CaH_4, the highest positive value of 1.49 1/fs was observed at 8.06 eV, while a negative response of −1.38 1/fs occurred at 3.71 eV. Similarly, the imaginary part of K_2MgH_4 reached a maximum positive value of 1.47 1/fs at 8.14 eV and decreased to a minimum of −2.42 1/fs at 4.55 eV. These findings indicate that both compounds display strong optical responses under high-energy photon excitation and may possess promising properties for optoelectronic applications, particularly in the ultraviolet (UV) region.

The refractive index $n(\omega)$ is a fundamental optical parameter that governs the propagation of light in a material and provides insight into its optical transparency and dispersion characteristics. In the static state, this quantity is defined by the relation $n(0) = \sqrt{\varepsilon_1\ (0)}$ [82]. The static refractive index was calculated as 1.77 for K_2MgH_4 and 1.70 for K_2CaH_4. According to the spectral distribution presented in Fig. 8(a), the maximum refractive index for K_2MgH_4 was found to be 2.39 at 4.52 eV. In contrast, the refractive index of K_2CaH_4 exhibited a first peak of 2.06 at 3.52 eV, followed by a second peak of 1.75 at 6.73 eV. These peaks are consistent with the parallel behavior observed between the $\varepsilon_1(\omega)$ and $n(\omega)$ functions, thereby supporting the reliability of the present calculations. Overall, the results reveal that the highest refractive index values for both compounds occur in the ultraviolet (UV) region.

The optical absorption coefficient $I(\omega)$ describes the extent to which a material absorbs light of a specific energy or wavelength [83]. Fig. 8(b) presents the energy-dependent optical absorption coefficient $I(\omega)$ curve of K_2XH_4 (X = Mg, Ca) compounds. Both materials exhibit high transparency in the 0–4.50 eV energy range, with no significant absorption observed in this region. As the photon energy increases, the absorption coefficient rises sharply due to electronic transitions from the valence band to the conduction band. For K_2MgH_4, the highest peak was observed at 9.48 eV with a value of approximately 1.55×10^5 cm^{-1}. In the case of K_2CaH_4, a particularly pronounced absorption peak appeared

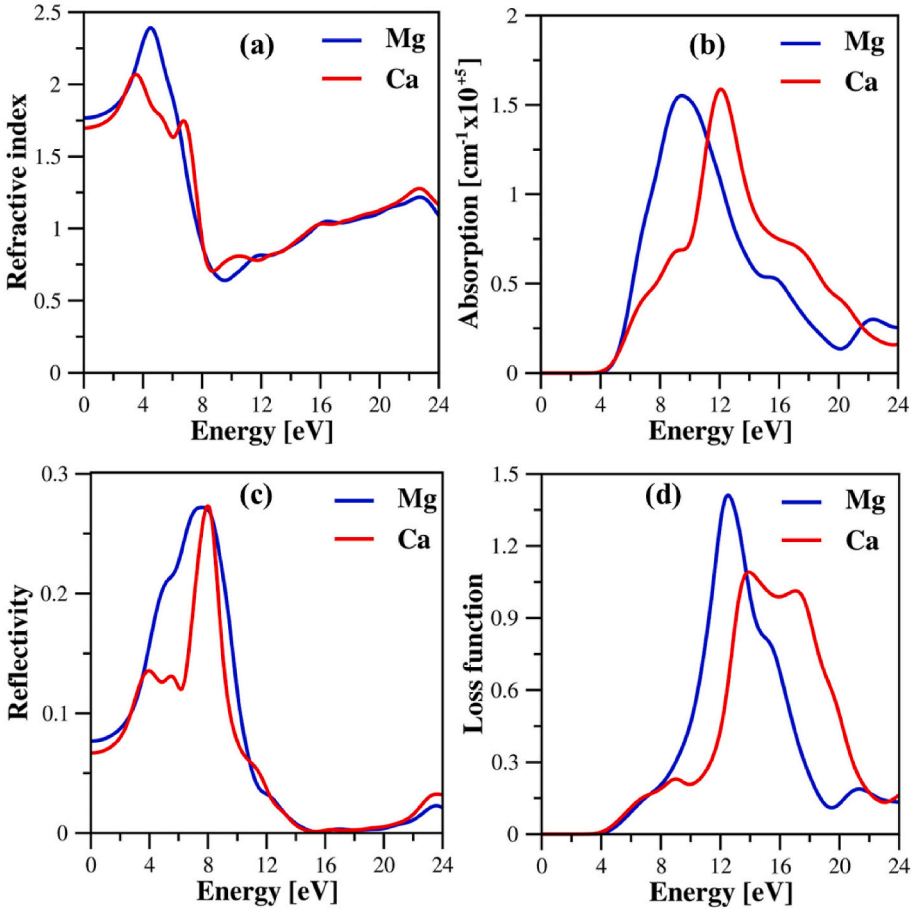

Fig. 8. (a) Refractive index, (b) Absorption coefficient, (c) Reflectivity, and (d) Loss function for K_2XH_4 (X = Mg, Ca).

at 12.10 eV, reaching approximately 1.58 × 10^5 cm^{-1}. These high absorption values demonstrate that K_2XH_4 hydrides can effectively absorb light in the ultraviolet (UV) region, suggesting that they may serve as promising candidates for photovoltaic and optoelectronic applications.

In addition, the reflectivity $R(\omega)$ is an important optical property that provides a quantitative measurement of the light radiation reflected from the surface of a material [84]. Fig. 8(c) shows the reflectance spectra of K_2XH_4 (X = Mg, Ca) compounds. The static reflectance values of these compounds were calculated as 0.077 and 0.067, respectively. A notable feature of the spectra is the maximum reflectance peaks observed at around 8 eV for both materials. These elevated reflectance values in the ultraviolet (UV) region indicate that K_2XH_4 compounds strongly interact with UV radiation, suggesting their potential use in optical coatings and UV-protective applications.

In addition to optical parameters such as reflectivity and absorption coefficient, the energy loss function $L(\omega)$ is a key metric for understanding how optical energy dissipates in a material through heat conversion and electron scattering [79,85]. Fig. 8(d) presents the energy loss spectra of K_2XH_4 (X = Mg, Ca) compounds. The calculations revealed maximum energy loss values of 1.41 at 12.53 eV for K_2MgH_4 and 1.08 at 13.90 eV for K_2CaH_4. These high-energy peaks in the ultraviolet (UV) region indicate that these hydrides strongly interact with high-energy photons and therefore may offer significant potential for optoelectronic applications.

3.7. Dynamic and thermodynamic properties

Fig. 9 shows the phonon dispersion curves and phonon density of states (PDOS) for the alkali metal hydrides (a) K_2MgH_4 and (b) K_2CaH_4. The presence of seven atoms per unit cells in these tetragonal structures results in a total of 21 phonon frequency branches [26]. For both compounds, the phonon frequencies extend up to 40 THz, and more importantly, no imaginary phonon frequencies are observed throughout the Brillouin zone, clearly confirming their dynamic stability. A detailed analysis of the vibrational modes reveals that the acoustic branches mainly originate from the collective motions of the heavier atoms (K, Mg, or Ca), whereas the high-frequency optical branches are predominantly associated with hydrogen vibrations. The PDOS further indicates that K and Mg/Ca atoms contribute to the low- and mid-frequency regions, while hydrogen vibrations dominate the high-frequency region above ~20 THz. The presence of a clear gap between the acoustic and optical regions indicates weak coupling between the heavy atoms and hydrogen atoms, further supporting the stability of these compounds. Overall, the absence of imaginary modes demonstrates that K_2XH_4 (X = Mg, Ca) compounds are dynamically stable, confirming their suitability as reliable candidates for hydrogen-related applications under operating conditions.

The thermodynamic properties of the K_2XH_4 (X = Mg, Ca) compounds were investigated within the framework of the quasi-harmonic Debye model [86,87]. As shown in Fig. 10, the free energy decreases with increasing temperature, while both the internal energy and entropy increase. The increase in entropy is more pronounced in K_2CaH_4, indicating a higher degree of disorder compared to K_2MgH_4, which may further facilitate hydrogen release. The heat capacity (C_V) is another key parameter for evaluating the vibrational properties and heat transfer capability of these compounds. At 300 K, the calculated (C_V) values are 129.02 J/mol.K for K_2CaH_4 and 110.76 J/mol.K for K_2MgH_4. At low temperatures (below 200 K), C_V exhibits a sharp increase, followed by a gradual saturation at higher temperatures, eventually approaching the Dulong–Petit limit of 171.92 J/mol.K [88]. This temperature-dependent

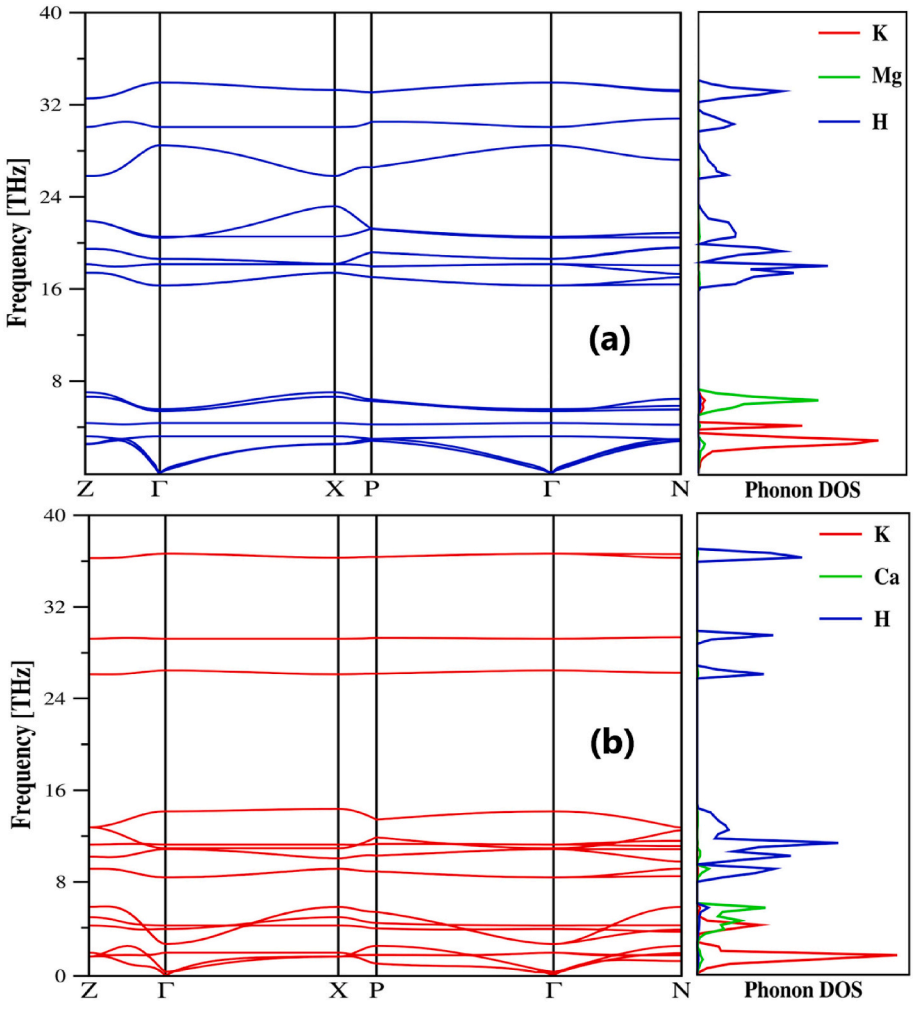

Fig. 9. The phonon dispersion curves and partial phonon density of states of (a) K_2MgH_4 and (b) K_2CaH_4.

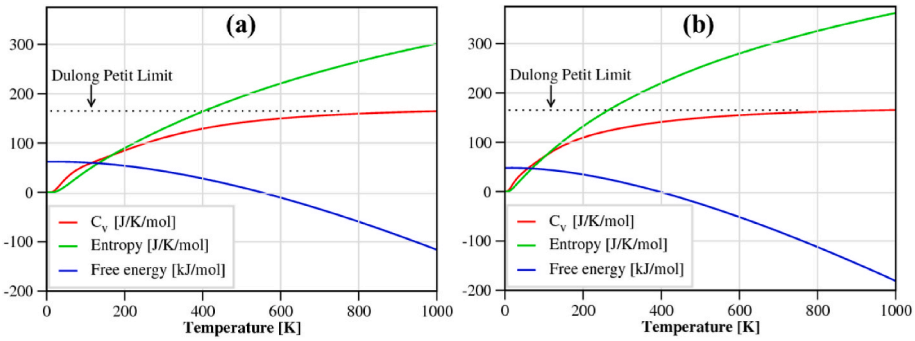

Fig. 10. The temperature dependencies of heat capacity, entropy, and free energy of (a) K_2MgH_4 and (b) K_2CaH_4.

trend provides valuable insights into the vibrational stability and thermal response of K_2XH_4 compounds.

Furthermore, zero-point energy (ZPE) refers to the quantum mechanical vibrational energy retained by a material even at absolute zero temperature (0 K) [89,90]. Originating primarily from the quantum vibrations of hydrogen atoms, ZPE plays a crucial role in evaluating the thermodynamic stability and hydrogen storage performance of complex hydrides. The calculated ZPE values are 62.08 kJ/mol (≈0.64 eV) for K_2MgH_4 and 48.08 kJ/mol (≈0.50 eV) for K_2CaH_4. The higher ZPE of K_2MgH_4 reflects stronger hydrogen vibrations and more dynamic H–metal interactions, favoring faster hydrogen release kinetics, whereas the lower ZPE of K_2CaH_4 implies weaker vibrational contributions and a more stable hydrogen environment, beneficial for maintaining structural integrity during hydrogen cycling. These complementary characteristics suggest that K_2MgH_4 offers kinetic advantages, while K_2CaH_4 provides thermodynamic robustness, making both compounds attractive candidates for solid-state hydrogen storage. The phonon dispersion and phonon DOS plots (Fig. 9) further support these findings, as K_2MgH_4 exhibits stronger high-frequency hydrogen modes, whereas K_2CaH_4 shows comparatively softer H vibrations. The absence of imaginary phonon modes in both cases confirms their dynamical stability and underlines their potential as reliable hydrogen storage materials

combining favorable vibrational properties with structural stability.

3.8. Debye temperature and thermal properties

Elastic properties are used to determine thermal parameters such as sound velocity (v_m, v_t, and v_l), Debye temperature (Θ_D), melting temperature (T_M), and Grüneisen parameter (γ) for K_2XH_4 (X = Mg, Ca), as summarized in Table 6. Debye temperature (Θ_D) is one of the fundamental parameters that determines the thermal conductivity of a material due to lattice vibrations. This quantity plays a critical role, especially in lattice dynamics and thermal conductivity calculations [91]. One of the common methods to determine the Debye temperature is to calculate it using the standard equation given below with elastic constants [92]:

$$\Theta_D = \frac{h}{k_B}\left[\frac{3n}{4\pi}\frac{\rho N_A}{M}\right]^{1/3} v_m \tag{14}$$

where h is Planck's constant, k_B Boltzmann's constant, n is the number of atoms in the molecule, ρ is the mass density, N_A is the Avogadro number, M is the mass of atoms contained in the unit cell, and v_m averaged sound velocity. The average sound velocity in the polycrystalline material is given [92,93]:

$$v_m = \left[\frac{1}{3}\left(\frac{2}{v_t^3}+\frac{1}{v_l^3}\right)\right]^{-1/3} \tag{15}$$

where v_t and v_l are the longitudinal and the transverse sound velocity. These are calculated in the following expressions of the Bulk modulus (B) and Shear modulus (G) by means of Navier equations [94]:

$$v_t = \sqrt{\frac{G}{\rho}} \quad and \quad v_l = \sqrt{\frac{3B+4G}{3\rho}} \tag{16}$$

The melting temperature of the K_2XH_4 compound was calculated by applying the equation given below:

$$T_M(K) = [553 + (5.91 \times C_{11})] \mp 300 \tag{17}$$

The Debye temperature (Θ_D) of K_2CaH_4 was calculated as 385.81 K, which reflects the energetic nature of its lattice vibrations and confirms its thermodynamic stability. In comparison, K_2MgH_4 exhibits a higher Debye temperature of 442.94 K, suggesting stronger lattice bonding and higher vibrational frequencies. The melting temperature (T_M) of K_2CaH_4 was determined as 558.41 K, slightly lower than that of K_2MgH_4 (569.59 K), indicating that the thermal resistance of K_2CaH_4 is more limited. Furthermore, the Grüneisen parameter (γ), which provides insight into the anharmonicity of lattice vibrations, was calculated as 1.39 for K_2CaH_4 and 1.28 for K_2MgH_4. The higher γ value of K_2CaH_4 suggests stronger anharmonic effects and higher lattice vibration amplitudes, implying a greater sensitivity to thermal fluctuations. These results collectively indicate that while both compounds are thermodynamically stable, K_2MgH_4 demonstrates stronger lattice stability, whereas K_2CaH_4 may be more suitable for applications operating in the low-to-medium-temperature range.

Ab initio molecular dynamics (AIMD) simulations were carried out for K_2MgH_4 and K_2CaH_4 at 300 K under the NVT ensemble for a total duration of 5000 fs [95,96]. As illustrated in Fig. 11(a) and 12(a), both compounds maintain nearly constant total energy with only minor fluctuations, confirming their structural robustness during the simulation. The corresponding temperature profiles in Fig. 11(b) and 12(b) remain stable around 300 K, further indicating thermal equilibrium without noticeable deviations. While K_2MgH_4 shows slightly smoother energy fluctuations compared to K_2CaH_4, both compounds preserve their crystalline integrity throughout the simulation. These results clearly demonstrate that K_2MgH_4 and K_2CaH_4 are dynamically and thermally stable at room temperature, consistent with previously reported AIMD studies on perovskite hydrides such as $XSnH_3$ (X = Rb, Cs, and Fr) [97]. Moreover, the absence of imaginary phonon modes, together with the AIMD simulations at 300 K, provides complementary evidence that both compounds are dynamically stable, further confirming their potential as reliable hydrogen storage materials. Therefore, these hydrides can be regarded as promising candidates for hydrogen storage and other energy-related applications owing to their combined dynamic and thermal stability. Particularly in hydrogen storage systems where thermal endurance is essential, our findings provide a solid theoretical basis supporting the practical applicability of K_2XH_4 (X = Mg, Ca) hydrides.

Thermal conductivity is one of the fundamental physical properties of a material that is directly related to the acoustic wave speeds and generally decreases as the temperature increases [98–100]. Therefore, determining the minimum thermal conductivity value is of critical importance for evaluating the performance of materials to be used, especially in high-temperature environments. For this purpose, various theoretical models have been developed in the literature to estimate the minimum thermal conductivity. In particular, the Cahill [101], Clarke [102], and Long [103] models are widely used to define the minimum thermal conductivity limits for solid materials. However, the Snyder [104] model allows the calculation of thermal conductivity based on the diffusion mechanism. In this study, the thermal conductivity properties of the alkali metal hydride K_2XH_4 (X = Mg, Ca) compounds were calculated using these theoretical models specified in Eqs. (18)–(22), and the findings are presented in Table 7.

Cahill model:

$$\lambda_{min} = \frac{k_B}{2.48} p^{2/3}(v_l + 2v_t) \tag{18}$$

Clarke model:

$$\lambda_{min} = 0.87 k_B M_a^{-3/2} E^{2/3} \rho^{1/6} \tag{19}$$

$$M_a = \left[\frac{M}{n.N_A}\right] \tag{20}$$

Long model:

$$\lambda_{min} = \left\{\frac{1}{3}\left[2(2+2\nu)^{3/2} + \left(\frac{1}{1-\nu}-\nu\right)^{3/2}\right]\right\}^{-1/3} k_B n^{2/3}\left(\frac{E}{\rho}\right)^{1/2} \tag{21}$$

Snyder model:

$$\lambda_{diff} = 0.76\, n^{2/3} k_B v_m \tag{22}$$

In these equations, ρ represents the density of the material, E represents the Young's modulus, p is the number of atoms per unit volume, and k_B represents the Boltzmann constant. The average atomic mass (M_a) is defined as the mass per atom in the crystal lattice, and this value is calculated using the molar mass M, Avogadro's number N_A, and the

Table 6
The calculated density (ρ), longitudinal wave velocity (v_l), transverse wave velocity (v_t), average wave velocity (v_m), Debye temperature (Θ_D), melting temperature (T_M), Grüneisen parameter (γ) of K_2XH_4 (X = Mg, Ca).

Compound	ρ (g/cm^3)	v_l (m/s)	v_t (m/s)	v_m (m/s)	Θ_D (K)	T_M	γ	*Ref.*
K_2MgH_4	1.587	5533	3391	3743	442.94	569.59	1.28	This work
	1.59	5372	3320	3662	433.00	552.55	1.25	[26]
K_2CaH_4	1.493	5288	3147	3484	385.81	558.41	1.39	This work

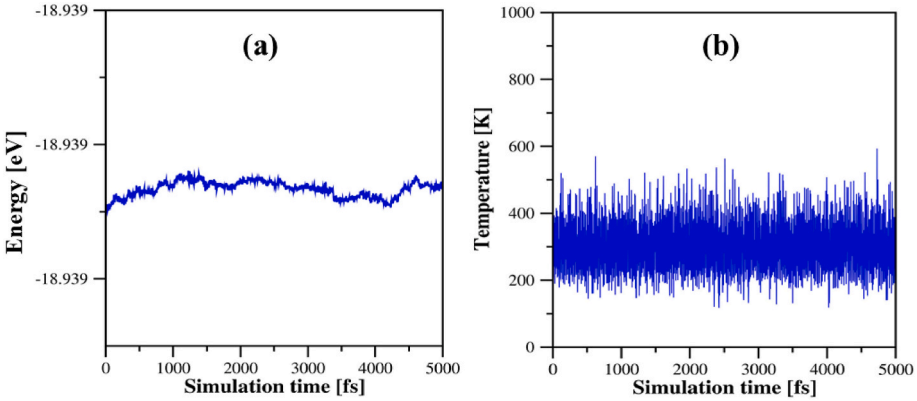

Fig. 11. The AIMD simulation of (a) energy and (b) temperature as a function of simulation time for K_2MgH_4.

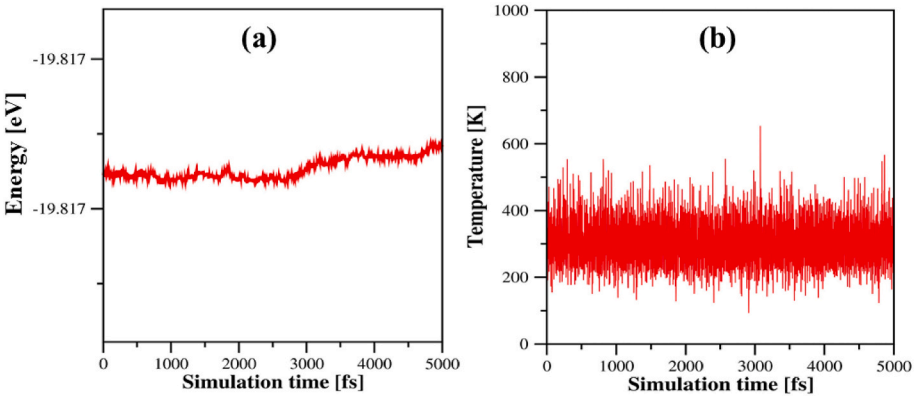

Fig. 12. The AIMD simulation of (a) energy and (b) temperature as a function of simulation time for K_2CaH_4.

Table 7
The calculated minimum thermal conductivity (λ_{min} in $W.m^{-1}K^{-1}$).

Compound	Clarke model		Cahill model		Long Model	Synder Model
	M_a (10^{-26})	λ_{min}	p (10^{28})	λ_{min}	λ_{min}	λ_{diff}
K_2MgH_4	2.527	0.996	6.279	1.083	0.657	0.621
K_2CaH_4	2.901	0.819	5.146	0.892	0.611	0.506

number of atoms in a molecule n. However, v_l and v_t are the longitudinal and transverse acoustic wave velocities, respectively, and v_m is the average wave velocity.

According to the minimum thermal conductivity values presented in Table 7, the calculated λ_{min} values for K_2MgH_4 are 0.996, 1.083, 0.657, and 0.621 W $m^{-1}K^{-1}$ based on the Clarke, Cahill, Long, and Snyder models, respectively. For K_2CaH_4, the corresponding values are 0.819, 0.892, 0.611, and 0.506 W $m^{-1}K^{-1}$. Among these, the Snyder model consistently predicts the lowest values for both compounds, reflecting a more diffusion-based mechanism of thermal transport. Comparatively, K_2CaH_4 shows slightly lower conductivity than K_2MgH_4, suggesting more effective thermal insulation. From a hydrogen storage perspective, such low thermal conductivities are advantageous as they help retain localized heat during hydrogen release, reducing external energy demand and improving storage efficiency. These findings provide the first theoretical estimates of λ_{min} for K_2XH_4 (X = Mg, Ca), highlighting their favorable thermal management properties and strengthening their potential as solid-state hydrogen storage materials.

4. Conclusion

In this study, the structural, mechanical, electronic, thermal, dynamic, and optical properties of K_2XH_4 (X = Mg, Ca) hydrides were systematically investigated using first-principles density functional theory. To begin with, the optimized lattice parameters of K_2MgH_4 are in excellent agreement with experimental data, while those of K_2CaH_4 are reported here for the first time. Furthermore, negative formation enthalpies confirm the thermodynamic stability of both compounds, with K_2CaH_4 being slightly more stable. In terms of mechanical behavior, stability was confirmed by elastic constants satisfying the Born criteria. Moreover, the calculated Bulk and Shear moduli indicate that K_2MgH_4 is slightly stiffer than K_2CaH_4, while negative Cauchy pressures and B/G ratios below 1.75 confirm their brittle character. Electronic structure calculations reveal semiconducting behavior, with wide band gaps of 3.43 eV (K_2MgH_4) and 3.41 eV (K_2CaH_4) at the PBE level, increasing to 4.67 eV and 4.60 eV, respectively, within the HSE06 functional. Consistently, the density of states analysis further indicates strong hybridization between metal and hydrogen orbitals. Regarding thermal and dynamic properties, analyses show Debye temperatures of 442.94 K for K_2MgH_4 and 385.81 K for K_2CaH_4 and melting points above 550 K confirming their thermal robustness. In addition, optical properties such as dielectric function, refractive index, and absorption coefficient reveal strong optical activity in the UV region. Regarding hydrogen storage performance, the calculated gravimetric capacities are 3.80 wt% for K_2MgH_4 and 3.30 wt% for K_2CaH_4, with corresponding desorption temperatures of 207.87 K and 254.88 K, respectively. While K_2CaH_4 falls within the DOE-recommended desorption temperature (233–333 K), and K_2MgH_4 falls below it, the gravimetric capacities of both compounds remain below the DOE 2025 ultimate target (~5.5 wt%), indicating that

further optimization will be required for practical use. Overall, these findings provide not only theoretical insights into the fundamental properties of K_2XH_4 (X = Mg, Ca) hydrides but also serve as practical guidance for future experimental studies aiming to develop efficient solid-state hydrogen storage materials.

CRediT authorship contribution statement

Abdullah Candan: Writing – review & editing, Writing – original draft, Visualization, Supervision, Software, Methodology, Investigation, Data curation. **Salih Akbudak:** Writing – review & editing, Writing – original draft, Visualization, Investigation, Formal analysis, Conceptualization.

Notes

The authors have declared no conflict of interest and have made an equal contribution to this study.

Declaration of competing interest

The authors declare that they have no known competing financial interests or personal relationships that could have appeared to influence the work reported in this paper.

Acknowledgments

This research was supported in part by TÜBİTAK (The Scientific & Technological Research Council of Turkey) through TR-Grid e-Infrastructure Project. Part of the calculations have been carried out at ULAKBİM Computer Center.

Data availability

Data will be made available on request.

References

[1] A.M. Omer, Energy use and environmental impacts: a general review, J. Renew. Sustain. Energy 1 (2009) 053101, https://doi.org/10.1063/1.3220701.
[2] A. Kalair, N. Abas, M.S. Saleem, A.R. Kalair, N. Khan, Role of energy storage systems in energy transition from fossil fuels to renewables, Energy Storage 3 (2021) e135, https://doi.org/10.1002/est2.135.
[3] M. Ganjian, M. Kolahdouz, A. Aletayeb, M. Norouzi, P. Ebrahimi, S. Pourjafari, M. S.S. Mousavi, ZnS shell-like CdS quantum dot-sensitized solar cell grown by SILAR approach; effect of electrolyte, counter electrode, and shell thickness, Vacuum 146 (2017) 548–553, https://doi.org/10.1016/j.vacuum.2017.02.007.
[4] H. Lei, Z. Wu, H. Wang, C. Mao, Z. Guo, L. Fei, W. Chen, Converting H_2O and CO_2 into chemical fuels by nickel via friction, Surf. Interfaces 46 (2024) 104203, https://doi.org/10.1016/j.surfin.2024.104203.
[5] M. Höök, X. Tang, Depletion of fossil fuels and anthropogenic climate change–A review, Energy Policy 52 (2013) 797–809, https://doi.org/10.1016/j.enpol.2012.10.046.
[6] V. Kanna, S. Roseline, K. Balamurugan, S. Jeeva, I.A. Santhiyagu, The effects of greenhouse gas emissions on global warming, Encyclopedia Renew. Energy Sustain. Environ. 1 (2024) 143–154.
[7] M. El-Adawy, I.B. Dalha, M.A. Ismael, Z.A. Al-Absi, M.A. Nemitallah, Review of sustainable hydrogen energy processes: production, storage, transportation, and color-coded classifications, Energy Fuel. 38 (2024) 22686–22718, https://doi.org/10.1021/acs.energyfuels.4c04317.
[8] N. Xu, R. Song, S. Chen, Y. Chen, S. Li, Z. Jiang, W. Zhang, First-principles study on the structure, mechanical, electrical, optical, kinetic, thermodynamic and hydrogen storage properties of the hydride perovskites $XScH_3$ (X = K, Rb, Cs) for hydrogen storage applications, J. Energy Storage 107 (2025) 114945, https://doi.org/10.1016/j.est.2024.114945.
[9] T. Tang, Y. Tang, First-principles calculations to investigate Mg_3XH_8 (X = Ca, Sc, Ti, V, Cr, Mn) materials for hydrogen storage, Int. J. Hydrogen Energy 74 (2024) 372–383, https://doi.org/10.1016/j.ijhydene.2024.06.052.
[10] A.M. Sadeq, R.Z. Homod, A.K. Hussein, H. Togun, A. Mahmoodi, et al., Hydrogen energy systems: technologies, trends, and future prospects, Sci. Total Environ. (2024) 173622, https://doi.org/10.1016/j.scitotenv.2024.173622.
[11] Q. Hassan, S. Algburi, A.Z. Sameen, M. Jaszczur, H.M. Salman, Hydrogen as an energy carrier: properties, storage methods, challenges, and future implications, Environ. Syst. Decis. 44 (2024) 327–350, https://doi.org/10.1007/s10669-023-09932-z.
[12] Y. Pan, J. Gao, Transition metal improved the dehydrogenated capacity, electronic and optical properties of the layered V_2C MXene for hydrogen evolution reaction, Surf. Interfaces 62 (2025) 106185, https://doi.org/10.1016/j.surfin.2025.106185.
[13] F. Yang, Y. Pan, I.P. Jain, Single atom enhanced the catalytic activity of borophene catalysts for hydrogen evolution reaction, Int. J. Hydrogen Energy 140 (2025) 223–232, https://doi.org/10.1016/j.ijhydene.2025.05.339.
[14] F. Yang, Y. Pan, J. Zhu, Enhanced catalytic activity of noble metal@borophene/WS_2 heterojunction for hydrogen evolution reaction, Appl. Surf. Sci. 680 (2025) 161321, https://doi.org/10.1016/j.apsusc.2024.161321.
[15] K. Locke, The urgency of hydrogen: environmental issues and the need for change, Futur. Sustain. 2 (2024) 46–58. https://fupubco.com/fusus/article/view/175.
[16] I. D'Adamo, M. Gastaldi, M. Giannini, A.S. Nizami, Environmental implications and levelized cost analysis of E-fuel production under photovoltaic energy, direct air capture, and hydrogen, Environ. Res. 246 (2024) 118163, https://doi.org/10.1016/j.envres.2024.118163.
[17] M.A. Aminudin, S.K. Kamarudin, B.H. Lim, E.H. Majilan, M.S. Masdar, N. Shaari, An overview: current progress on hydrogen fuel cell vehicles, Int. J. Hydrogen Energy 48 (2023) 4371–4388, https://doi.org/10.1016/j.ijhydene.2022.10.156.
[18] A. Züttel, M. Hirscher, B. Panella, K. Yvon, S.I. Orimo, B. Bogdanović, M.T. Kelly, Hydrogen storage, in: Hydrogen as a Future Energy Carrier, Wiley-VCH, Weinheim, 2008, pp. 165–263, https://doi.org/10.1002/9783527622894.
[19] D. Khan, W.J. Ong, Tailoring hydrogen storage materials kinetics and thermodynamics through nanostructuring, and nanoconfinement with in-situ catalysis, Interdiscip. Mater. 4 (2025) 249–283, https://doi.org/10.1002/idm2.12234.
[20] M. Lavanya, S. Shrivastava, T. Lakshmi, E.R. Sandadi, S. Gour, N.A. Thomas, K. Sudhakar, An overview of hydrogen storage technologies – key challenges and opportunities, Mater. Chem. Phys. (2024) 129710, https://doi.org/10.1016/j.matchemphys.2024.129710.
[21] K. Naseem, F. Qin, F. Khalid, G. Suo, T. Zahra, Z. Chen, Z. Javed, Essential parts of hydrogen economy: hydrogen production, storage, transportation and application, Renew. Sustain. Energy Rev. 210 (2025) 115196, https://doi.org/10.1016/j.rser.2024.115196.
[22] Y. Pan, F. Yang, Structural, hydrogen storage capacity, electronic and optical properties of Li–N–H hydrogen storage materials from first-principles investigation, J. Energy Storage 87 (2024) 111492, https://doi.org/10.1016/j.est.2024.111492.
[23] Y. Pan, J. Gao, Exploring the hydrogen storage capacity, dehydrogenated mechanism, electronic and optical properties of $AMMgH_3$ hydrides for hydrogen storage, J. Energy Storage 124 (2025) 116869, https://doi.org/10.1016/j.est.2025.116869.
[24] J. Gao, Y. Pan, I.P. Jain, F. Yang, J. Zhu, Exploring the structure, hydrogen storage capacity and hydrogen storage mechanism of $X_3N_3H_6$ hydrides for hydrogen storage, Appl. Mater. Today 44 (2025) 102755, https://doi.org/10.1016/j.apmt.2025.102755.
[25] T. Tang, Y. Tang, Lithium doping in Na-based double perovskite for hydrogen storage and improving their optoelectronic properties: first-principles investigation, Mater. Chem. Phys. 316 (2024) 129099, https://doi.org/10.1016/j.matchemphys.2024.129099.
[26] Ç. Yamçıçıer, Exploring the structural, elastic, phonon, optoelectronics, and thermoelectric properties of tetragonal complex metal hydride X_2MgH_4 (X = K, Rb, and Cs) compounds for hydrogen storage applications, Int. J. Hydrogen Energy 48 (2023) 39930–39943, https://doi.org/10.1016/j.ijhydene.2023.09.177.
[27] H.H. Raza, M. Naeem, H.S. Ali, A. Parveen, A.M. Al-Enizi, First-principles investigation of BX_3H_9 (X = Ca, Sc, Ti) hydrides: structural, electronic, phonon, and hydrogen storage properties, J. Phys. Chem. Solid. (2025) 112800, https://doi.org/10.1016/j.jpcs.2025.112800.
[28] C. Soykan, C. Kürkçü, First-principles calculations to investigate structural, electronic, mechanical, optical, vibrational, thermal properties, and hydrogen storage capabilities of Rb_2SnH_4 for hydrogen storage applications, J. Phys. Chem. Solid. (2025) 112618, https://doi.org/10.1016/j.jpcs.2025.112618.
[29] B. Bertheville, P. Fischer, K. Yvon, High-pressure synthesis and crystal structures of new ternary caesium magnesium hydrides, $CsMgH_3$, $Cs_4Mg_3H_{10}$ and Cs_2MgH_4, J. Alloys Compd. 330 (2002) 152–156, https://doi.org/10.1016/S0925-8388(01)01631-0.
[30] Z.Z. Wang, Y.F. Wang, B.Y. Tang, X.Q. Zeng, W.J. Ding, Theoretical study of the $CsMgH_3$, Cs_2MgH_4 and $Cs_4Mg_3H_{10}$ complex hydrides from first-principles, Phys. Status Solidi B 245 (2008) 2749–2755, https://doi.org/10.1002/pssb.200743355.
[31] A. Assila, M. Rkhis, A. Alaoui-Belghiti, S. Laasri, E.K. Hlil, Y. Boughaleb, A. Hajjaji, Feeling the strain: enhancing the thermodynamics characteristics of magnesium nickel hydride Mg_2NiH_4 for hydrogen storage applications through strain engineering, Int. J. Hydrogen Energy 67 (2024) 651–657, https://doi.org/10.1016/j.ijhydene.2024.04.159.
[32] B. Ahmed, M.B. Tahir, A. Dahshan, M. Sagir, Advanced computational screening of X_2CaH_4 (X = Rb and Cs) for hydrogen storage applications, Int. J. Hydrogen Energy 89 (2024) 48–55, https://doi.org/10.1016/j.ijhydene.2024.09.321.
[33] M. Ali, Z. Bibi, M.W. Younis, K. Majeed, U. Afzal, S. Khan, M. Mubashir, Enhancement of hydrogen storage characteristics of Na_2CaH_4 hydrides by introducing the Mg and be dopant: a first-principles study, Int. J. Hydrogen Energy 70 (2024) 579–590, https://doi.org/10.1016/j.ijhydene.2024.05.169.

[34] S. Azam, Q. Rafiq, E.R. Elsharkawy, M.T. Khan, S.M. El-Bahy, W. Khan, S.A. Khan, First-principles investigation of Rb_2CaH_4 and Cs-doped Rb_2CaH_4: unveiling their potential for hydrogen storage through mechanical and optoelectronic properties, Int. J. Hydrogen Energy 116 (2025) 462–472, https://doi.org/10.1016/j.ijhydene.2025.03.083.

[35] B. Bertheville, T. Herrmannsdörfer, K. Yvon, Structure data for K_2MgH_4 and Rb_2CaH_4 and comparison with hydride and fluoride analogues, J. Alloys Compd. 325 (2001) L13–L16, https://doi.org/10.1016/S0925-8388(01)01368-8.

[36] H.P. Rodenburg, D. Koops, K. Peinecke, V. Kyriakou, P. Ngene, Synthesis, hydrogen sorption properties, and hydride-ion conductivity of K_2MgH_4, ACS Appl. Energy Mater. 8 (2025) 875–882, https://doi.org/10.1021/acsaem.4c02359.

[37] D. Liu, K. Cao, J. Huang, J. Zhang, R. Sa, Theoretical evaluation of the hydrogen storage, mechanical, and optoelectronic properties of antiperovskites $X_3H(ZnH_4)$ (X = Na, K, Rb, Cs), Int. J. Hydrogen Energy 113 (2025) 190–197, https://doi.org/10.1016/j.ijhydene.2025.02.477.

[38] H.U. Rehman, N. Muhammad, G. Murtaza, H.H. Raza, S.M. Ramay, M. Irfan, M. A. Rehman, The investigation of structural, electronic, thermal, and elastic properties of X_2ZnH_4 (X = K, Rb and Cs) for hydrogen storage applications: DFT study, Opt. Quant. Electron. 56 (2024) 636, https://doi.org/10.1007/s11082-024-06308-8.

[39] G. Kresse, J. Hafner, Ab initio molecular dynamics for liquid metals, Phys. Rev. B 47 (1993) 558–561, https://doi.org/10.1103/PhysRevB.47.558.

[40] G. Kresse, J. Furthmüller, Efficiency of ab initio total energy calculations for metals and semiconductors using a plane-wave basis set, Comput. Mater. Sci. 6 (1996) 15–50, https://doi.org/10.1016/0927-0256(96)00008-0.

[41] P.E. Blöchl, Projector augmented-wave method, Phys. Rev. B 50 (1994) 17953–17979, https://doi.org/10.1103/PhysRevB.50.17953.

[42] J.P. Perdew, K. Burke, M. Ernzerhof, Generalized gradient approximation made simple, Phys. Rev. Lett. 77 (1996) 3865–3868, https://doi.org/10.1103/PhysRevLett.77.3865.

[43] J. Paier, M. Marsman, K. Hummer, G. Kresse, I.C. Gerber, J.G. Ángyán, Screened hybrid density functionals applied to solids, J. Chem. Phys. 124 (2006) 154709, https://doi.org/10.1063/1.2187006.

[44] H.J. Monkhorst, J.D. Pack, Special points for Brillouin-zone integrations, Phys. Rev. B 13 (1976) 5188, https://doi.org/10.1103/PhysRevB.13.5188.

[45] Y. Le Page, P. Saxe, Symmetry-general least-squares extraction of elastic data for strained materials from ab initio calculations of stress, Phys. Rev. B 65 (2002) 104104, https://doi.org/10.1103/PhysRevB.65.104104.

[46] A. Togo, First-principles phonon calculations with phonopy and phono3py, J. Phys. Soc. Jpn. 92 (2023) 012001, https://doi.org/10.7566/JPSJ.92.012001.

[47] G. Marius, The Physics of Semiconductors: Kramers–Kronig Relations, Springer, Berlin Heidelberg, 2010, pp. 775–776.

[48] M. Ishfaq, M. Yaseen, S. Shukrullah, S. Noreen, Optoelectronic and thermoelectric transport phenomena in Sr_2LaTaO_6 and Sr_2LuTaO_6 double perovskites, Mater. Chem. Phys. 313 (2024) 128728, https://doi.org/10.1016/j.matchemphys.2023.128728.

[49] S. Jamshaid, S.A. Aldaghfag, M.K. Butt, M. Yaseen, A. Murtaza, M. Ishfaq, H. H. Hegazy, Investigation of cubic K_2NaXBr_6 (X = Sc, Y) double perovskites for optical and thermoelectric devices, J. Phys. Chem. Solid. 178 (2023) 111341, https://doi.org/10.1016/j.jpcs.2023.111341.

[50] F. Birch, Finite elastic strain of cubic crystals, Phys. Rev. 71 (1947) 809, https://doi.org/10.1103/PhysRev.71.809.

[51] H.H. Raza, G. Murtaza, M. Shafiq, S.A. Shakoor, First-principles calculations on structural, mechanical and thermodynamic properties of orthorhombic Mg_2BeTMH_8 (TM = Ni, Cu and Zn) for hydrogen storage applications, Int. J. Hydrogen Energy 62 (2024) 637–651, https://doi.org/10.1016/j.ijhydene.2024.03.127.

[52] Y. Song, Z.X. Guo, R.J. Yang, Influence of selected alloying elements on the stability of magnesium dihydride for hydrogen storage applications: a first-principles investigation, Phys. Rev. B 69 (2004) 094205, https://doi.org/10.1103/PhysRevB.69.094205.

[53] A. Ayyaz, M.A. Ullah, M. Zaman, N.D. Alkhaldi, Q. Mahmood, I. Boukhris, M. S. Al-Buriahi, M.M. Al-Anazy, Investigation of hydrogen storage and energy harvesting potential of double perovskite hydrides A_2LiCuH_6 (A = Be/Mg/Ca/Sr): a DFT approach, Int. J. Hydrogen Energy 102 (2025) 1329–1339, https://doi.org/10.1016/j.ijhydene.2025.01.117.

[54] A. Candan, A. Erkisi, B. Yildiz, Revealing the potential of double perovskite hydrides A_2SiH_6 (A = Li, Na) for solid-state hydrogen storage applications, J. Energy Storage 132 (2025) 117957, https://doi.org/10.1016/j.est.2025.117957.

[55] M. Baaddi, R. Chami, O. Baalla, S.E. Quaoubi, A. Saadi, L.E.H. Omari, M. Chafi, The effect of strain on hydrogen storage characteristics in K_2NaAlH_6 double perovskite hydride through first principle method, Environ. Sci. Pollut. Res. 31 (2024) 62056–62064, https://doi.org/10.1007/s11356-023-27529-6.

[56] A. Candan, S. Akbudak, First-principles calculations on the physical properties of Zr-based perovskites $LiZrH_3$ and $KZrH_3$ for potential hydrogen storage applications, Int. J. Hydrogen Energy 129 (2025) 199–210, https://doi.org/10.1016/j.ijhydene.2025.04.189.

[57] H. Daglar, H.C. Gulbalkan, G.O. Aksu, S. Keskin, Computational simulations of metal–organic frameworks to enhance adsorption applications, Adv. Mater. (2024) 2405532, https://doi.org/10.1002/adma.202405532.

[58] S. Bahou, H. Labrim, M. Lakhal, M. Bhihi, B. Hartiti, H. Ez-Zahraouy, Magnesium vacancies and hydrogen doping in MgH_2 for improving gravimetric capacity and desorption temperature, Int. J. Hydrogen Energy 46 (2021) 2322–2329, https://doi.org/10.1016/j.ijhydene.2020.10.078.

[59] A. Arharbi, H. Jebari, H. Ez-Zahraouy, New insights from DFT analysis: mg vacancies and hydrogen doping in enhancing thermodynamic properties and hydrogen storage performance of Li_2BeMgH_6, J. Energy Storage 106 (2025) 114903, https://doi.org/10.1016/j.est.2024.114903.

[60] A. Quader, M. Kiran, A. Bakar, M. Ahmed, Y. Khairy, Density functional analysis of structural, mechanical, electronic, and hydrogen storage properties of thermodynamically stable lead-free hydrides $XGeH_3$ (X = Cs, Fr): a perspective of clean energy and fuel, Int. J. Hydrogen Energy 85 (2024) 652–660, https://doi.org/10.1016/j.ijhydene.2024.08.399.

[61] R.A. Alabdulhadi, S. Khan, A. Khan, L.T. Alfuhaid, M.Y. Khan, M. Usman, A. Helal, Potential use of reticular materials (MOFs, ZIFs, and COFs) for hydrogen storage, ACS Appl. Energy Mater. 8 (2025) 1397–1413, https://doi.org/10.1021/acsaem.4c02317.

[62] M. Born, On the stability of crystal lattices. I, Math. Proc. Camb. Philos. Soc. 36 (1940) 160–172, https://doi.org/10.1017/S0305004100017138.

[63] L. Yang, Y. Cao, Z. Xu, N. Qu, First-principles prediction of hydrogen storage capabilities in Pd-based alkali metal hydride X_2PdH_4 (X = Na, K, Rb, and Cs), Int. J. Hydrogen Energy 100 (2025) 444–455, https://doi.org/10.1016/j.ijhydene.2024.12.318.

[64] D.G. Pettifor, Theoretical predictions of structure and related properties of intermetallics, Mater. Sci. Technol. 8 (1992) 345–349, https://doi.org/10.1179/mst.1992.8.4.345.

[65] G. Surucu, A. Gencer, A. Candan, H.H. Gullu, M. Isik, $CaXH_3$ (X = Mn, Fe, Co) perovskite-type hydrides for hydrogen storage applications, Int. J. Energy Res. 44 (2020) 2345–2354, https://doi.org/10.1002/er.5062.

[66] A. Candan, M. Kurban, Electronic structure, elastic and phonon properties of perovskite-type hydrides $MgXH_3$ (X = Fe, Co) for hydrogen storage, Solid State Commun. 281 (2018) 38–43, https://doi.org/10.1016/j.ssc.2018.07.004.

[67] W. Voigt, Lehrbuch der Kristallphysik (Textbook of Crystal Physics), BG Teubner, Leipzig und Berlin, 1928.

[68] A. Reuß, Berechnung der Fließgrenze von Mischkristallen auf Grund der Plastizitätsbedingung für Einkristalle, ZAMM–J. Appl. Math. Mech. 9 (1929) 49–58, https://doi.org/10.1002/zamm.19290090104.

[69] R. Hill, The elastic behaviour of a crystalline aggregate, Proc. Phys. Soc. 65 (1952) 349, https://doi.org/10.1088/0370-1298/65/5/307.

[70] E. Deligoz, D. Rached, H. Ozisik, M. Caid, Y. Rached, Lead-free Na_2ZrTeO_6 double perovskite: a promising candidate for high-temperature and optoelectronic applications, Adv. Theory Simul. (2025) 2401421, https://doi.org/10.1002/adts.202401421.

[71] S.F. Pugh, XCII. Relations between the elastic moduli and the plastic properties of polycrystalline pure metals, Philos. Mag. 45 (1954) 823–843, https://doi.org/10.1080/14786440808520496.

[72] V.V. Bannikov, I.R. Shein, A.L. Ivanovskii, Electronic structure, chemical bonding and elastic properties of the first thorium-containing nitride perovskite $TaThN_3$, Phys. Status Solidi RRL 1 (2007) 89–91, https://doi.org/10.1002/pssr.200600116.

[73] P. Gogoi, S. Deb, Silver nanoparticles decorated wide band gap MoS_2 nanosheet: enhanced optical and electrical properties, Plasmonics 20 (2025) 575–583, https://doi.org/10.1007/s11468-024-02253-0.

[74] X. Zhou, Z. Lu, L. Zhang, Q. Ke, Wide-bandgap all-inorganic lead-free perovskites for ultraviolet photodetectors, Nano Energy 117 (2023) 108908, https://doi.org/10.1016/j.nanoen.2023.108908.

[75] W. Khan, The first principles insights of aluminum-based hydrides for hydrogen storage application, Int. J. Hydrogen Energy 63 (2024) 596–608, https://doi.org/10.1016/j.ijhydene.2024.03.180.

[76] G. Henkelman, A. Arnaldsson, H. Jónsson, A fast and robust algorithm for Bader decomposition of charge density, Comput. Mater. Sci. 36 (2006) 354–360, https://doi.org/10.1016/j.commatsci.2005.04.010.

[77] R.F. Bader, Atoms in molecules, Acc. Chem. Res. 18 (1985) 9–15.

[78] R.K. Pan, J.G. Yao, R.L. Ji, W.W. Liu, D.F. Yin, First principles study on elastic and electronic properties of bialkali alanates $M_2M'AlH_6$, Int. J. Hydrogen Energy 43 (2018) 3862–3870, https://doi.org/10.1016/j.ijhydene.2018.01.006.

[79] W. Khan, First principles study of chromium-based hydrides for optoelectronics and hydrogen storage applications, J. Phys. Chem. Solid. 192 (2024) 112068, https://doi.org/10.1016/j.jpcs.2024.112068.

[80] S. Sharma, M. Jahanzaib, J. Lee, D. Park, Nanomaterial/nanocomposite for green energy application, in: Nanomaterials as a Catalyst for Biofuel Production, Springer Nature Singapore, Singapore, 2025, pp. 271–293, https://doi.org/10.1007/978-981-96-1706-7_11.

[81] A. Candan, A.K. Kushwaha, A first-principles study of the structural, electronic, optical, and vibrational properties for paramagnetic half-Heusler compound TiIrBi by GGA and GGA + mBJ functional, Mater. Today Commun. 27 (2021) 102246, https://doi.org/10.1016/j.mtcomm.2021.102246.

[82] Q. Mahmood, T. Ghrib, A. Rached, A. Laref, M.A. Kamran, Probing of mechanical, optical and thermoelectric characteristics of double perovskites Cs_2GeCl_6/Br_6 by DFT method, Mater. Sci. Semicond. Process. 112 (2020) 105009, https://doi.org/10.1016/j.mssp.2020.105009.

[83] M.R. Kabli, J. Ur Rehman, M.B. Tahir, M. Usman, A.M. Ali, K. Shahzad, Structural, electronics and optical properties of sodium-based fluoroperovskites $NaXF_3$ (X = Ca, Mg, Sr and Zn): first principles calculations, Phys. Lett. 412 (2021) 127574, https://doi.org/10.1016/j.physleta.2021.127574.

[84] K. Bougherara, S. Al-Qaisi, A. Laref, T.V. Vu, D.P. Rai, Ab initio insight of the electronic, structural, mechanical and optical properties of X_3P_2 (X = Mg, Ca) from GGA and hybrid functional (HSE06), J. Supercond. Nov. Magn. 35 (2022) 79–86, https://doi.org/10.1007/s10948-021-06009-3.

[85] M.A. Rehman, J. Fatima, Z.U. Rehman, S.Y. Alomar, M. Sohiab, A. Hamad, The DFT study of the structural, hydrogen, electronic, mechanical, thermal, and optical properties of KXH_3 (X = Ca, Sc, Ti, & Ni) perovskites for H_2 storage applications, Struct. Chem. 36 (2025) 235–248, https://doi.org/10.1007/s11224-024-02362-w.

[86] M.A. Blanco, E. Francisco, V.G.I. Luana, GIBBS: isothermal-isobaric thermodynamics of solids from energy curves using a quasi-harmonic Debye model, Comput. Phys. Commun. 158 (2004) 57–72, https://doi.org/10.1016/j.comphy.2003.12.001.

[87] S. Daoud, N. Bioud, P.K. Saini, Finite temperature thermophysical properties of MgCu intermetallic compound from quasi-harmonic Debye model, J. Magnes. Alloys 7 (2019) 335–344, https://doi.org/10.1016/j.jma.2019.01.006.

[88] P.L. Dulong, A.T. Petit, Recherches sur quelques points importans de la théorie de la Chaleur, 1819.

[89] M. Archi, O. Bajjou, K. Rahmani, B. Elhadadi, Investigation of structural, phonon, thermodynamic, electronic, and mechanical properties of non-toxic $XZnH_3$ (X = Li, Na, K) perovskites for solid-state hydrogen storage: a DFT and AIMD approach, J. Energy Storage 112 (2025) 115492, https://doi.org/10.1016/j.est.2025.115492.

[90] M. Archi, O. Bajjou, B. Elhadadi, A comparative ab initio analysis of the stability, electronic, thermodynamic, mechanical, and hydrogen storage properties of $SrZnH_3$ and $SrLiH_3$ perovskite hydrides through DFT and AIMD approaches, Int. J. Hydrogen Energy 105 (2025) 759–770, https://doi.org/10.1016/j.ijhydene.2025.01.312.

[91] G. Surucu, A. Candan, A. Gencer, M. Isik, First-principle investigation for the hydrogen storage properties of $NaXH_3$ (X = Mn, Fe, Co) perovskite-type hydrides, Int. J. Hydrogen Energy 44 (2019) 30218–30225, https://doi.org/10.1016/j.ijhydene.2019.09.201.

[92] O.L. Anderson, A simplified method for calculating the Debye temperature from elastic constants, J. Phys. Chem. Solid. 24 (1963) 909–917, https://doi.org/10.1016/0022-3697(63)90067-2.

[93] N. Miao, B. Sa, J. Zhou, Z. Sun, Theoretical investigation on the transition-metal borides with Ta_3B_4-type structure: a class of hard and refractory materials, Comput. Mater. Sci. 50 (2011) 1559–1566, https://doi.org/10.1016/j.commatsci.2010.12.015.

[94] E. Schreiber, O.L. Anderson, N. Soga, Elastic Constants and Their Measurement, McGraw-Hill, New York, 1974, https://doi.org/10.1115/1.3423687.

[95] D.W. Boukhvalov, I.S. Zhidkov, A.F. Akbulatov, A.I. Kukharenko, S.O. Cholakh, K. J. Stevenson, E.Z. Kurmaev, Thermal effects and halide mixing of hybrid perovskites: MD and XPS studies, J. Phys. Chem. A 124 (2019) 135–140, https://doi.org/10.1021/acs.jpca.9b09653.

[96] Z. Li, X. Yang, Y. Yang, X. Li, Y. Gao, L. Wang, W. Lü, Enhanced Li-ion battery performance based on multisite oxygen vacancies in WO_{3-x}@rGO negative electrode, Chem. Eng. J. 498 (2024) 155383, https://doi.org/10.1016/j.cej.2024.155383.

[97] M.K. Masood, W. Khan, K. Chaoui, Z. Ashraf, S. Bibi, A. Kanwal, J. Rehman, Theoretical investigation of $XSnH_3$ (X = Rb, Cs, Fr) perovskite hydrides for hydrogen storage application, Int. J. Hydrogen Energy 63 (2024) 1248–1257, https://doi.org/10.1016/j.ijhydene.2024.03.229.

[98] E. Deligoz, H. Ozisik, E. Bolen, Physical insights on the ultralow thermal conductivity of Ag_8XSe_6 (X = Si, Ge, and Sn), Inorg. Chem. Commun. 142 (2022) 109689, https://doi.org/10.1016/j.inoche.2022.109689.

[99] A.L. Ding, C.M. Li, J. Wang, J. Ao, F. Li, Z.Q. Chen, Anisotropy of elasticity and minimum thermal conductivity of monocrystal M_4AlC_3 (M = Ti, Zr, Hf), Chin. Phys. B 23 (2014) 096201, https://doi.org/10.1088/1674-1056/23/9/096201.

[100] A. Gencer, O. Surucu, G. Surucu, E. Deligoz, Anisotropic mechanical properties of $Tl_4Ag_{18}Te_{11}$ compound with low thermal conductivity, J. Solid State Chem. 289 (2020) 121469, https://doi.org/10.1016/j.jssc.2020.121469.

[101] D.G. Cahill, S.K. Watson, R.O. Pohl, Lower limit to the thermal conductivity of disordered crystals, Phys. Rev. B 46 (1992) 6131–6140, https://doi.org/10.1103/PhysRevB.46.6131.

[102] D.R. Clarke, C.G. Levi, Materials design for the next generation thermal barrier coatings, Annu. Rev. Mater. Res. 33 (2003) 383–417, https://doi.org/10.1146/annurev.matsci.33.011403.113718.

[103] J. Long, C. Shu, L. Yang, M. Yang, Predicting crystal structures and physical properties of novel superhard p-BN under pressure via first-principles investigation, J. Alloys Compd. 644 (2015) 638–644, https://doi.org/10.1016/j.jallcom.2015.04.229.

[104] M.T. Agne, R. Hanus, G.J. Snyder, Minimum thermal conductivity in the context of diffuson-mediated thermal transport, Energy Environ. Sci. 11 (2018) 609–616, https://doi.org/10.1039/C7EE03256K.